Measurement report: Comprehensive Seasonal Study of the

2 Composition and Sources of Submicron Aerosol during the

3 JULIAC Campaign in Germany

- 4 Lu Liu^{1,2}, Thorsten Hohaus¹, Andreas Hofzumahaus¹, Frank Holland¹, Hendrik Fuchs^{1,3}, Ralf Tillmann¹, Birger
- 5 Bohn¹, Stefanie Andres¹, Zhaofeng Tan^{1, 4}, Franz Rohrer¹, Vlassis A. Karydis¹, Vaishali Vardhan^{1, 5}, Philipp
- 6 Franke¹, Anne C. Lange¹, Anna Novelli¹, Benjamin Winter¹, Changmin Cho^{1, 6}, Iulia Gensch¹, Sergej Wedel¹,
- 7 Andreas Wahner¹, and Astrid Kiendler-Scharr^{1,#}
- 8 ¹ Institute of Climate and Energy Systems, ICE-3: Troposphere, Forschungszentrum Jülich GmbH, Jülich,
- 9 Germany
- 10 ² now at: Center for Energy and Environmental Sciences, Paul Scherrer Institute, Villigen, Switzerland
- 11 ³ Department of Physics, University of Cologne, Cologne, Germany
- ⁴ now at: College of Environmental Sciences and Engineering, Peking University, Beijing, China
- 13 ⁵ now at: Environmental Research Institute, University College Cork, Cork, Ireland
- 14 ⁶ now at: Atmospheric Chemistry Observations & Modeling (ACOM), National Center for Atmospheric
- 15 Research (NCAR), Boulder, USA
- 16 # deceased
- 17 Correspondence to: Lu Liu (<u>lu.liu1@psi.ch</u>), and Thorsten Hohaus (<u>t.hohaus@fz-juelich.de</u>)
- 18
- 19 Abstract. The seasonal variations of aerosol sources and their atmospheric evolution are investigated using
- 20 observations from the year-long JULIAC (Jülich Atmospheric Chemistry Project) campaign (January-
- 21 November 2019) in Jülich, Germany. Non-refractory submicron aerosol components were continuously
- measured alongside oxidants (OH, O₃, NO₃), trace gases, and meteorological conditions. Organic aerosols (OA)
- dominated the aerosol composition throughout the year (39–58%), with secondary formation being the major
- 24 source. OA, including organic nitrate and organosulfate, peaked during a summer heatwave event due to
- 25 enhanced daytime and nighttime secondary OA formation driven by elevated concentrations of atmospheric
- oxidants. Changes in the OA composition during the heatwave suggest a shift in the formation pathways, where
- isoprene may play an important role. Biomass-burning, mainly wildfires and anthropogenic activities (e.g.,
- heating, industry), is the dominant primary OA source (45–83%), which may grow in influence due to climate
- 29 change and the expected energy transition. Air masses containing OA from regional transport from marine and
- 30 wildfire sources are identified through source apportionment. Analysis and modeling prove this method to be
- 31 more reliable than traditional tracer-based methods. Regional transport to this study site typically shows a
- 32 cleansing effect on the aerosol concentration, except in winter. Furthermore, seasonal variations in the effects of
- 33 regional transport are seen, where identical transport pathways led to different influences on aerosol properties,

driven by seasonal differences in biogenic and anthropogenic emissions. This study enhances understanding of seasonal variation in submicron aerosol properties in response to their sources, atmospheric evolution, and transport.

1 Introduction

34

35

36

37

68

69

70

38 Atmospheric submicron aerosols affect air quality, climate-ecology interaction (Boucher et al., 2013; 39 Ramanathan et al., 2001), and also human health (Dockery et al., 1993; Dockery and Stone, 2007; Pope and 40 Dockery, 2006; Lelieveld et al., 2015). The chemical and physical properties of aerosols change according to 41 diverse primary emissions, secondary formations, and their chemical transformation (e.g., oligomerization, 42 fragmentation, photochemical aging) in the atmosphere (Canagaratna et al., 2010; Jimenez et al., 2009; Ng et al., 43 2010). Hence, their climate impact varies through direct scattering and absorption of radiation and indirect 44 modification of cloud properties as cloud condensation nuclei (CCN) (Fanourgakis et al., 2019; Myhre et al., 45 2013). Therefore, understanding aerosol emissions and secondary formation is essential, as these processes 46 determine aerosol properties and how they influence radiation and clouds, altering climate impacts. 47 Among submicron aerosol compounds, organic aerosols (OA) contribute 20% to 90% of the total submicron 48 aerosol mass in the troposphere (Zhang et al., 2007; Jimenez et al., 2009), thus playing a key role in altering the 49 environmental impact of aerosols. OA can be emitted directly from primary sources, including anthropogenic 50 activities (e.g., residential heating, traffic exhaust) and biogenic sources (e.g., wildfire). Additionally, abundant 51 secondary OA (SOA) forms predominantly via atmospheric oxidation of various biogenic and anthropogenic 52 volatile organic compounds (VOCs) by different oxidants (OH, O₃, and NO₃). For example, the particulate 53 organic nitrate, as a typical secondary species mainly formed via NO₃ oxidation (Xu et al., 2015b; Lee et al., 54 2016), has been shown to contribute 34% to 44% of measured submicron aerosol nitrate on a continental scale 55 (Kiendler-Scharr et al., 2016). Organosulfate, another important SOA component, which is essential for 56 determining aerosol physicochemical properties, affects the formation of CCN (Chen et al., 2019). However, 57 sources of organosulfate in the atmosphere are diverse, originating from both gas-phase (Yang et al., 2023) and 58 liquid-phase chemistry (Tan et al., 2022a). While the prevailing view has been that interactions between 59 anthropogenic and biogenic sources primarily contribute to the formation of organosulfate, a recent study 60 (Bruggemann et al., 2020) suggests that reactions of purely anthropogenic precursor species or direct emissions 61 from fossil fuel and biomass-burning may contribute significantly to the formation of organosulfate. 62 Nevertheless, the sources and formation mechanisms of organosulfates remain uncertain and require further 63 studies. 64 To investigate the complex sources and evolution of OA, receptor models are commonly used to analyze the OA 65 composition, identifying several source factors. These factors primarily include primary OA (POA) components, 66 as well as oxidized OA (OOA) formed through secondary oxidation, as shown in Figure 1. Previous ambient 67 studies aiming to identify sources primarily attributed OOA formation to photochemical processes (Hildebrandt

et al., 2010; Jimenez et al., 2009; Sun et al., 2012; Kostenidou et al., 2015), like less oxidized oxygenated OA

demonstrated significant OOA production from nocturnal chemistry (Fry et al., 2009; Ng et al., 2008), which

(LO-OOA) and more oxidized oxygenated OA (MO-OOA) in Figure 1. However, laboratory experiments have

has also been supported by model simulations (Hoyle et al., 2007; Pye et al., 2010; Russell, 2005). Observational studies further suggest night-time OOA formation, as evidenced by observations of the enhancement of oxidized OA during the night (Saarikoski et al., 2012; Crippa et al., 2013; Florou et al., 2017; Cheng et al., 2021). The study by Liu et al. (2024), which investigates data from the JULIAC (Jülich Atmospheric Chemistry Project) campaign, highlights nocturnal OOA formation (marked as NO-OOA in Figure 1) from NO₃ oxidation during all seasons.

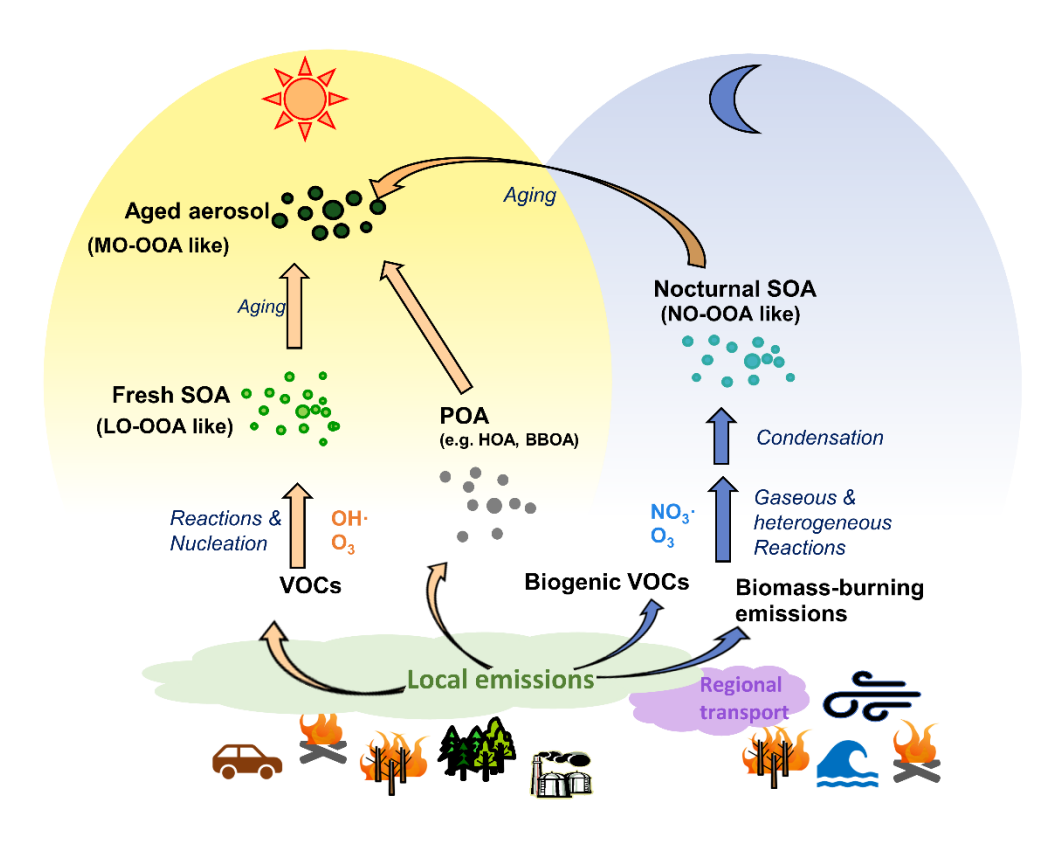


Figure 1: Overview of sources and evolution processes of OA identified in this study.

In addition to local primary emissions and secondary formation, long-term regional transport affects atmospheric conditions as well as aerosol properties. For example, methanesulfonic acid (MSA, CH₃SO₃H) is widely regarded as a tracer for marine air transport because its precursor, dimethyl sulfide (Zorn et al., 2008; Ge et al., 2012), is primarily produced by phytoplankton and anaerobic bacteria in the ocean (Charlson et al., 1987). Regional transport carries MSA inland or to higher altitudes, shaping its atmospheric concentration and distribution, which in turn can influence CCN activity and climate (Yan et al., 2019). Methanesulfonic acid-containing organic aerosol (MSA-OA) has been resolved in previous studies, not only in the coastal and oceanic environments (Schmale et al., 2013), but also at continental sites (Crippa et al., 2014).

Several studies (Hass-Mitchell et al., 2024; Otu-Larbi et al., 2020; Ma et al., 2019) have analysed that strong SOA formation is associated with intensive photochemistry during heatwave events with coincident elevated O₃ and biogenic VOCs (mainly isoprene) concentrations. However, the detailed changes in aerosol properties and the dominant SOA formation mechanism are less frequently discussed. In this multi-seasonal study, an

unusually warm summer is observed, which is reported as the third warmest summer in Germany over the past 39 years (Matzarakis et al., 2020). Notably, the abnormal heatwave lasts ten days, with ambient air temperatures reaching 36.6°C at 50 m above ground. The continuous measurement during the heatwave provides a valuable case study for understanding changes in SOA formation under shifts in VOCs emissions due to heat and drought stress of vegetation. In this study, comprehensive measurements and analyses are conducted to investigate the seasonal variations in aerosol composition, with a particular focus on OA contributions from local primary emissions, secondary formation, and long-range regional transport. Building upon the study of Liu et al. (2024), this study provides a more detailed analysis of the seasonal variations of NO-OOA formation from the perspective of its precursors. Special attention is given to the summer period, when a significant heatwave event occurred.

2 Methodology

2.1 Campaign site and setup

The JULIAC campaign, conducted from January to November 2019 at Forschungszentrum Jülich, Germany (50.91N, 6.41E), aimed to understand annual variations of atmospheric oxidant concentrations (Cho et al., 2023), the composition of gas-phase species (Tan et al., 2022b), and submicron aerosols (Liu et al., 2024). Intensive measurements were conducted during four periods in the different seasons: winter (JULIAC-I: 15 January – 10 February), spring (JULIAC-II: 8 April – 5 May), summer (JULIAC-III: 7 August – 1 September), and autumn (JULIAC-IV: 28 October – 24 November). The site, near a mixed forest and various anthropogenic sources such as a coal-fired power plant and a sugar factory, is influenced by both biogenic and anthropogenic emissions. During the JULIAC campaign, ambient air was sampled from 50 m height into the SAPHIR atmospheric chamber (Simulation of Atmospheric Photochemistry in a Large Reaction Chamber) (Bohn and Zilken, 2005; Bohn et al., 2005) and then analyzed by instruments connected to the chamber, minimizing the influence from local near-ground emissions, so that the air was representative of the region. Instruments measured radicals (e.g., OH, HO₂, RO₂)(Cho et al., 2023), trace gases, OH reactivity, submicron aerosol components, and the aerosol size distribution.

2.2 Instrumentations

The physical and chemical properties of ambient submicron aerosol were measured using an Aerodyne aerosol high-resolution time-of-flight aerosol mass spectrometer (HR-ToF-AMS), a scanning mobility particle sizer (SMPS 3080, TSI), and a condensation particle counter (CPC 3788, TSI). The HR-ToF-AMS provided continuous measurements of mass concentrations and size distributions for non-refractory chemical components of the aerosol (e.g., ammonium, nitrate, sulfate, chlorine, and organics). Comprehensive descriptions of the maintenance and data processing of HR-ToF-AMS in this study are provided in prior studies (Liu et al., 2022, 2024). In brief, ionization calibrations were conducted biweekly throughout the campaign using an ammonium nitrate standard following Drewnick et al. (2005). The relative ionization efficiency (RIE) of species was also determined every two weeks using ammonium sulfate, following Jimenez et al. (2003), and the RIE values applied for each campaign phase are summarized in Table S1. The AMS collection efficiency (CE) was

128 constrained by comparison with concurrent SMPS measurements, assuming an average aerosol density of 1.4 g 129 cm⁻³ (Cross et al., 2007). A constant CE of 0.96 was applied for JULIAC-I and II, whereas a composition-130 dependent CE (Middlebrook et al., 2012) with a value of 0.57 was used for JULIAC-III and IV. One flow rate 131 correction was performed during JULIAC-II by comparing the AMS flow (derived from the lens pressure) with 132 flow rate measurements obtained using a Gilibrator. The SMPS scanned particles in the 10-750 nm range with a 133 7-minute cycle, while a standalone CPC recorded total particle concentrations (diameter >5 nm). N₂O₅ 134 concentrations were measured by custom-built cavity ring-down spectroscopy (FZJ-CRDS), which is similar to 135 the instrument described in Wagner et al. (2011), and CO, CO₂, and CH₄ were detected by a commercial cavity 136 ring-down instrument (Picarro, G2401). Nitrogen oxides (NO and NO₂) were detected using a 137 chemiluminescence instrument with a photolytic converter (ECO PHYSICS), while O3 levels were measured with two UV photometers (Ansyco 41M and Thermo Scientific 49i), both of which showed good agreement 138 139 (within 5%). VOCs were monitored with a proton transfer reaction-time of flight mass spectrometer (PTR-ToF-140 MS). For the PTR-ToF-MS, the drift tube was operated at an E/N of 126 Td during JULIAC I and II and 141 adjusted to 120 Td during JULIAC III and IV. The PTR was calibrated on a weekly basis whenever possible. 142 For calibration, the instrument was connected to our Liquid Calibration Unit (LCU), and a multi-step calibration 143 was performed using a gas standard at ~60% relative humidity. We used four concentration steps and one zero 144 step (five steps in total), with the standard diluted in the range of 1–15 ppb. The list of VOCs included in the 145 calibration standard, along with their mixing ratios and uncertainties, is provided in Table S2. A 146 spectroradiometer measured spectral actinic flux densities to determine photolysis frequencies (Bohn and 147 Zilken, 2005; Bohn et al., 2005). OH, HO₂, and RO₂ radicals were measured using the FZJ laser-induced 148 fluorescence (LIF) instrument (Cho et al., 2021), and the total OH reactivity (k(OH)) was measured using a 149 laser-flash photolysis LIF instrument (Fuchs et al., 2017). Additional sensors, such as an ultrasonic anemometer 150 (METEK, USA-1) and humidity, temperature, and pressure sensors (Driesen + Kern) monitored ambient 3D wind data, relative humidity (RH), temperature, and pressure at 50 m above ground and inside the chamber. 151 152 Further details on data quality and instrument performance during the JULIAC campaign are provided in Cho et 153 al. (2023).

2.3 Calculation of particulate organic nitrate and organosulfate concentrations

154

159

160

161

162

163

164

The concentration of particulate organic nitrate was calculated by an approach using nitrate fragment ratios (NO₂+/NO+) as shown in Eq. (1) based on HR-ToF-AMS measurements (Kiendler-Scharr et al., 2016; Farmer et al., 2010; Fry et al., 2013; Xu et al., 2015a).

$$pOrgNO_{3,frac} = \frac{(1 + R_{OrgNO3}) \times (R_{measured} - R_{calib})}{(1 + R_{measured}) \times (R_{OrgNO3} - R_{calib})}$$
(1)

 $R_{measured}$ represents the ratio of NO_2^+ to NO^+ ion fragments for aerosol measurements during the JULIAC campaign. R_{calib} represents the corresponding NO_2^+/NO^+ fragment ratio measured from ammonium nitrate during biweekly calibrations of the ionization efficiency (IE) of HR-ToF-AMS during the campaign, while R_{OrgNO3} stands for that ratio for pure organic nitrate, with a value of 0.1 suggested by Kiendler-Scharr et al. (2016). Based on this method, lower-limit estimations of organic nitrate concentrations having an uncertainty of \pm 20% (Xu et al., 2015a; Kiendler-Scharr et al., 2016) were reported in this study.

$$pOrgNO_{3,conc} = pOrgNpO_{3,frac} \times NO_{3,total}$$
 (2)

Particulate organosulfate concentrations were calculated from total sulfates measured by the HR-ToF-AMS using the sulfate fragment pattern method (Chen et al., 2019). The organosulfate calculation method makes use of the varying degrees of fragmentation of ammonium sulfate, MSA, and organosulfate during AMS measurements, resulting in differences in the distribution of fragments, including SO^{+,} SO₂⁺, SO₃⁺, HSO₃⁺, and H₂SO₄⁺. This method used in this study assumes that the fragment of H₂SO₄⁺ is exclusively contributed by ammonium sulfate, while the fragment of HSO₃⁺ originates from only ammonium sulfate and MSA. Then, the mass concentrations of total sulfate measured by the instrument ToF-AMS could be distributed to the sulfate from ammonium sulfate, MSA, and organosulfate, as shown below:

[SO₄]_(Ammonium Sulfate) =
$$\frac{H_2SO_4^{\dagger}}{f(H_2SO_4^{\dagger})_{Ammonium Sulfate} \cdot \Sigma HSO} \cdot [SO_4]$$
 (3)

$$[SO_4]_{(MSA)} = \frac{(HSO_3^{\dagger} - [SO_4]_{(Ammonium \, Sulfate)} \cdot f(HSO_3^{\dagger})_{Ammonium \, Sulfate)}}{f(HSO_3^{\dagger})_{MSA} \cdot \Sigma \, HSO} \cdot [SO_4]$$
(4)

$$[SO4](Organosulfate) = [SO4] - [SO4](Ammonium Sulfate) - [SO4](MSA)$$
(5)

- 177 Σ HSO represents the sum of molar concentrations of fragments of SO^{+,} SO₂⁺, SO₃⁺, HSO₃⁺, and H₂SO₄⁺.
- $f(H_2SO_4^+)_{Ammonium\ Sulfate}\ and\ f(HSO_3^+)_{Ammonium\ Sulfate}\ are\ the\ molar\ fractions\ of\ H_2SO_4^+\ and\ HSO_3^+\ normalized$
- to Σ HSO for ammonium sulfate, which was measured during biweekly calibrations of the IE of the HR-ToF-
- AMS instrument during the JULIAC campaign. Similarly, $f(HSO_3^+)_{MSA}$ stands for the molar fraction of HSO_3^+
- normalized to the Σ HSO concentration for pure MSA. The value of $f(HSO_3^+)_{MSA} = 0.0587$ reported by Chen et
- al. (2019) was used in this study, as their work showed a similar ammonium sulfate fragment distribution to
- ours. However, the study by Schueneman et al. (2021) points out that this method described above is not always
- reliable for identifying organosulfate. Based on that, the feasibility of this sulfate fragment pattern method is
- further discussed in Section 3.

166

167

168

169

170

171

172

173

186

2.4 PMF analysis

Positive matrix factorization (PMF) is applied to attribute the concentrations of aerosol components to various sources (Jimenez et al., 2009; Zhang et al., 2011; Sun et al., 2012; Dai et al., 2019; Crippa et al., 2014). PMF analysis decomposes the variability of a dataset X into a matrix of factor profiles F (source profiles) and a corresponding time series matrix G (source contributions) as shown in Eq. (6). Matrix E represents residuals not attributed to any source. The PMF algorithm minimizes the sum of squared residuals e_{ij} weighted by the uncertainty σ_{ij} for all input points in X, indicated by Q as shown in Eq. (7).

$$X = G \times F + E \tag{6}$$

$$Q = \sum_{i=1}^{m} \sum_{j=1}^{n} \left(\frac{e_{ij}}{\sigma_{ij}}\right)^{2}$$
 (7)

To investigate seasonal variations in the sources and contributions of OA, PMF analysis was performed separately for each season on OA concentrations (mass to charge ratio, m/z 12–160) measured by HR-ToFAMS during the JULIAC campaign. The SoFi Pro software (version 8.0.3.1) (Canonaco et al., 2013) was used

to control the multilinear engine (ME-2) algorithm (Paatero, 1999) for aerosol source apportionment, allowing for the incorporation of prior mass spectral information (Table S3-S5) to reduce rotational ambiguity (Paatero and Hopke, 2003). A signal-to-noise (S/N) threshold of 2 was applied, and down-weighting was used for S/N values below 1 to reduce errors. Factors identified in prior studies were used as references or for constraining the PMF analysis. The SoFi panel's criteria-based selection function was employed to explore similar results based on user-defined criteria, such as correlations with relevant trace gases (e.g., CO for biomass-burning sources). The optimal PMF solution was selected based on the evaluation of parameters, residuals, factor spectra, correlations with external tracers (e.g., VOCs, radicals, wind direction), and the interpretability of the factor's variation patterns. This involved assessing key parameters (e.g., Unexplained variation (UEV)) in Table S6, characteristics of source mass spectra (Tables S2–S4), and examining the agreement between resolved source factors with their diurnal patterns, related tracer, and atmospheric conditions (Fig. S1-S2).

2.5 Trajectory model

To understand the effect of long-term regional transport on aerosol properties, 24-h and 72-h backward trajectories with GDAS 1° and a 2-hour resolution from the sampling site were computed during the four JULIAC intensive phases using the HYSPLIT model (Version 5.0.0)(Stein et al., 2015), based on GDAS meteorological data from NOAA's Air Resources Laboratory (ARL). The trajectory arrival times match the detection times of instruments at the JULIAC campaign, with the trajectory endpoints set at 50 m above ground level. This altitude corresponds with the height of the sampling tube inlet of ambient air to the SAPHIR chamber. Further analyses, like cluster analysis and concentration field (CF) statistics (Seibert et al., 1994; Debevec et al., 2017), were performed using the ZeFir graphical interface (version 3.7) in Igor Pro (Petit et al., 2017). Additional details on ZeFir's trajectory analysis applications are available in previous studies (Debevec et al., 2021).

2.6 Aerosol liquid water content estimation

The aerosol liquid water content (ALWC) was estimated using the reverse mode of the ISORROPIA-II thermodynamic model (Fountoukis and Nenes, 2007). It uses measured ambient RH, temperature, and aerosol-phase concentrations to infer gas-phase species and predict thermodynamic equilibrium. This approach is advantageous when gas-phase precursors are unavailable, as in our dataset. By contrast, the forward mode of ISORROPIA-II requires both gas- and aerosol-phase inputs to simulate aerosol composition. However, previous evaluations have demonstrated strong consistency in the ALWC between the two modes for major aerosol components. The study of Fountoukis and Nenes (2007) reported normalized mean errors of $3.4 \pm 1.1\%$ for aqueous sulfate and $2.5 \pm 1.3\%$ for aqueous nitrate, which are the main drivers of ALWC. Since ALWC primarily scales with total aerosol mass, it is relatively insensitive to gas-phase constraints; accordingly, Guo et al. (2015) observed nearly identical ALWC predictions in both modes (slope = 0.993, intercept = $-0.005~\mu g~m^{-3}$, $R^2 = 0.99$). Consequently, relying on the reverse mode ALWC is a solid approach.

234 3 Results

235

236

237

238239

240

241

242

243

244

245

246

247

248

249

250

The variations of non-refractory chemical component concentrations of submicron aerosol (NF-PM₁), including organics, nitrate, ammonium, chlorine, and sulfate, were measured during each season of the JULIAC campaign. As shown in Table 1, the highest average concentration of NF-PM1 is observed in summer (JULIAC-III) (to be $7.7 \pm 4.8 \,\mu\text{g/m}^3$), which is more than seven times higher than the lowest concentration recorded in winter (JULIAC-I) (with $1.1 \pm 1.0 \,\mu\text{g/m}^3$). The annual average concentration of NF-PM₁ is $4.0 \,\mu\text{g/m}^3$ at this semi-rural site, similar to aerosol levels reported in previous studies in Europe and the United States of America (Table 1). In general, OA are the major component, accounting for 39% to 58% of the total mass of submicron aerosols. Aerosol sulfate (16%-26%) is the second most abundant component, followed by nitrate (5%-26%). The mass fractions of aerosol nitrate and organics show distinct seasonal patterns. During summer, nitrate contributes only about 5% of the total aerosol mass, substantially lower than the 23%-26% observed in other seasons, due to its high volatility. In contrast, OA contributes a much higher fraction in summer (58%) than in the other seasons (ranging from 39% to 58%), indicating a pronounced seasonal enhancement. The sulfate fraction remains relatively constant (20%-26%) throughout the year. To better understand these trends in aerosol composition and concentration, we conduct a detailed comparison of the properties of OA in each season. Additionally, the contributions of organic nitrate and organosulfate are estimated to evaluate the seasonal formation processes contributing to these aerosol species.

251

252

253

254

Table 1 Overview of the seasonal average concentrations of components of submicron aerosol measured by HR-ToF-AMS, together with atmospheric conditions (RH, and ambient temperature) during the four JULIAC intensive phases, compared with previous field observations.

Campaign	Total aerosol (μg·m ⁻³)	Nitrate (μg·m ⁻³)	Sulfate (μg·m ⁻³)	Ammonium (μg·m ⁻³)	Chlorine (μg·m ⁻³)	Organics (μg·m ⁻³)	RH (%)	Temp (°C)	Reference
JULIAC-I, Jan-Feb, 2019	1.1 ± 1.0	0.3±0.4	0.2±0.2	0.1±0.2	0.02±0.02	0.4±0.3	66±18	5±4	This study
JULIAC-II, Apr-May 2019	2.6 ± 2.6	0.6±1.3	0.5±0.4	0.4±0.5	0.02±0.02	1.1±0.9	44±21	12±6	This study
JULIAC-III, Aug- Sep 2019	7.7 ±4.8	0.4±0.5	2.0±1.2	0.8±0.5	0.02±0.01	4.4±3.0	45±21	21±5	This study
JULIAC-IV, Nov 2019	4.2 ± 2.3	1.0±0.8	0.7±0.4	0.5±0.3	0.04±0.03	2.0±1.1	65±15	15±5	This study
Cabauw, the Netherlands, Jul 2012-Jun 2013	6.2	1.9	0.9	0.9	0.06	2.2	82	9	(Schlag et al., 2016)

<u>Hyytiälä,</u> Finland, Mar-Apr 2005	2.0	0.3	0.3	0.2		1.2			(Raatikainen et al., 2010)
Texas, Houston, USA, Feb 2014	6.1±4.3	1.4±1.4	1.4±0.8	0.9±0.6	0.06±0.09	2.3±1.4	76±18	9±6	(Dai et al., 2019)
Texas, Houston, USA, May 2014	3.6±2.3	0.1±0.1	1.3±0.6	0.5±0.2	0.02±0.02	1.7±1.4	72±19	24±4	(Dai et al., 2019)
Oklahoma, USA, Nov 2010-Jul 2012	7.0±9.3	1.5±3.0	0.8±1.0	0.7±1.2	0.02±0.04	4.0±6.2			(Parworth et al., 2015)



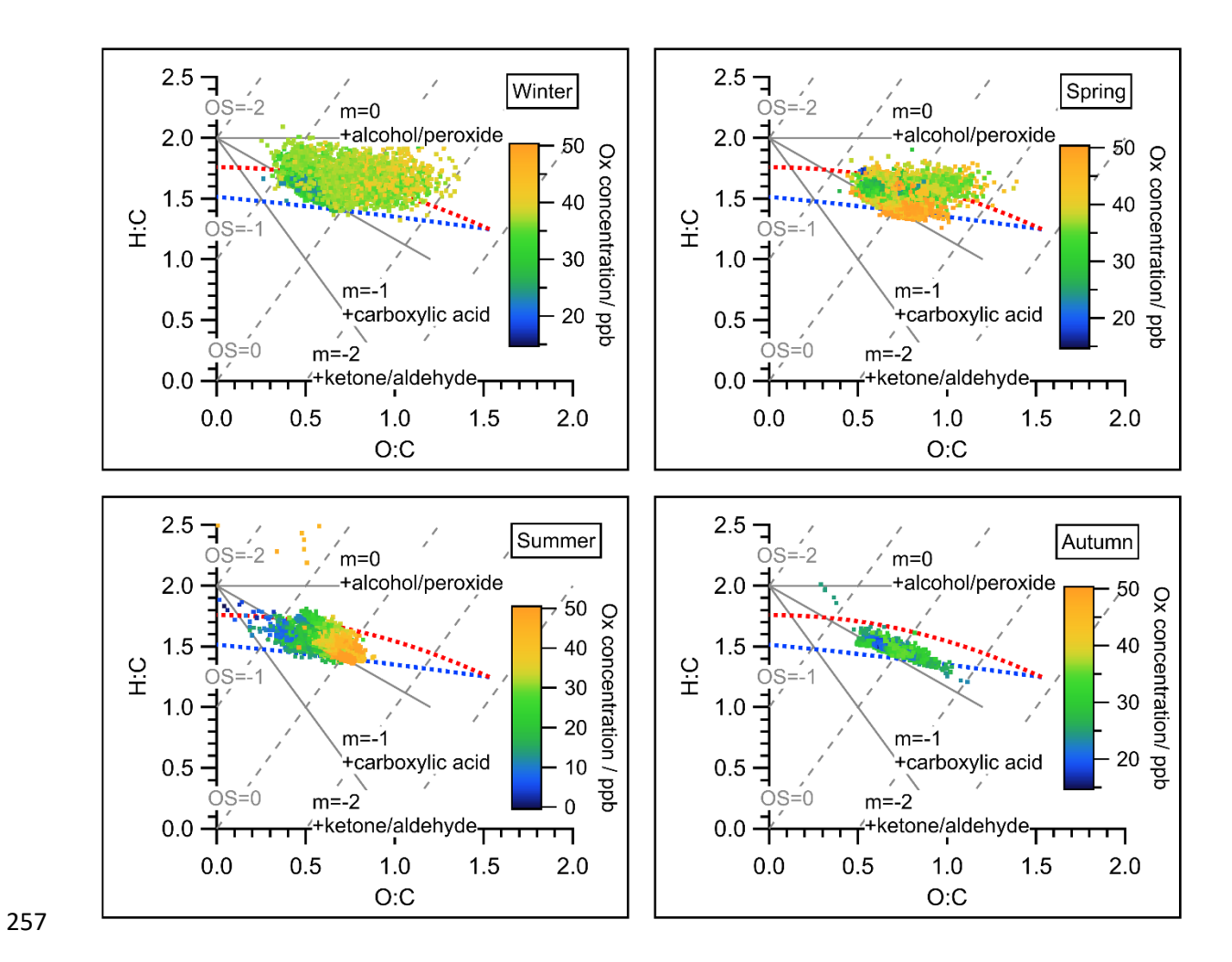
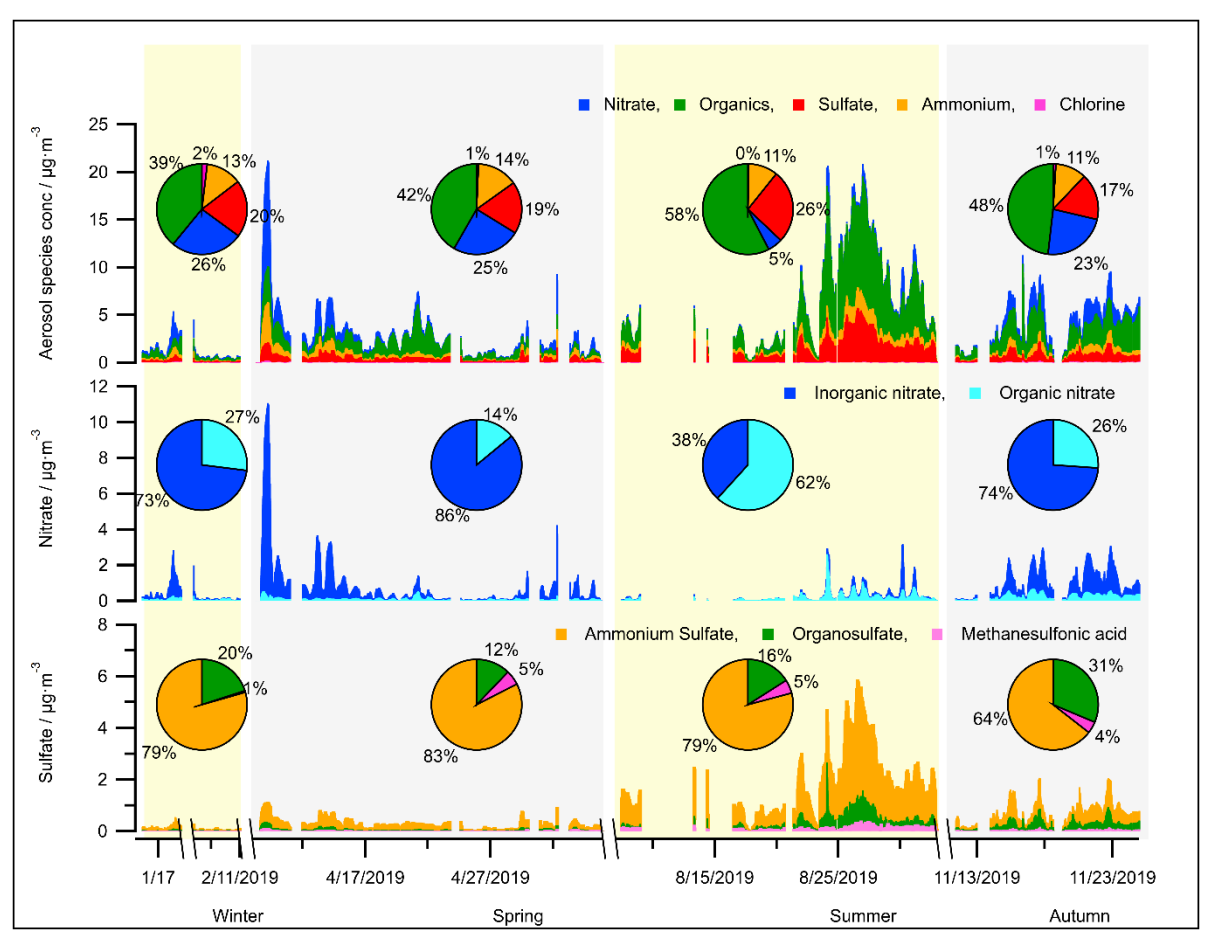


Figure 2: Van Krevelen triangle graph for all measurements of OA during the four seasons of the JULIAC campaign. Atomic ratio regions of standard groups for alcohol/peroxide, carboxylic acid, and ketone/aldehyde (Aiken et al., 2007) were marked as references. The dots in all graphs were color-coded by the concentration of the oxidant Ox (NO₂+O₃) to represent the intensity of secondary oxidation. The red and blue dashed line corresponds to the right and left lines of the f44/f43 triangle introduced in Ng et al. (2010), representing the lower oxidation level (like POA) and higher oxidation level (like SOA),

OA dynamically evolves in the atmosphere, converging to a higher oxidation status with time (Ng et al., 2011), which can be indicated by a high elemental O:C ratio or estimated carbon oxidation states (OSc≈2O/C-H/C) (Canagaratna et al., 2015). Hence, the oxidation degree of OA is a key parameter for understanding the atmospheric evolution of OA. In Figure 2, the degrees of oxidation of OA during each season are displayed in a Van Krevelen triangle (Ng et al., 2011), color-coded with O_X concentrations. O_x, defined as the sum of O₃ and nitrogen dioxide (NO₂), is a conserved quantity under photochemical cycling and is often used as a proxy for atmospheric oxidation capacity and, consequently, the intensity of secondary oxidation in the atmosphere (Li et al., 2015; Canonaco et al., 2015). During summer, the strongest correlation between the O:C ratios of OA and the Ox concentrations is observed, suggesting the significant contribution of SOA formation to total OA. This assumption is further discussed and supported by the results of the source apportionment analysis presented in Section 4.1. The average oxidation degrees of OA for each season are calculated (Table S7). The overall oxidation degree of OA reaches the minimum during summer with an average O:C of 0.64 and the maximum in spring with an average O:C equal to 0.76. The difference in OA properties originates from the difference in emission sources and SOA formation mechanisms among seasons, which will be confirmed by the aerosol source apportionment analysis below (Section 4.1).



285 ammonium, chlorine) and calculated concentrations of species (organic nitrate, organosulfate, 286 methanesulfonic acid) from HR-ToF-AMS measurements. 287 Particulate organic nitrates have been reported as ubiquitous components and significant contributors to OA 288 mass in both Europe and the United States of America (Kiendler-Scharr et al., 2016; Ng et al., 2017). In this 289 study, a high mass fraction of organic nitrate to total aerosol nitrate, up to 62%, is found during the summer 290 (JULIAC-III) (Figure 3). This is not the first time that a high mass fraction of organic nitrate has been observed 291 in the European area. For instance, the fraction of organic nitrate to total aerosol nitrate was found to be 67% at 292 Cabauw, Netherlands in March 2008, 73% at Melpitz, Germany in March 2009, 63% at Harwell, UK in October 293 2008, and 67% at Vavihill, Sweden in October 2008 (Kiendler-Scharr et al., 2016). In this previous study based 294 on combined analyses of chemistry transport models, abundant organic nitrate is found to be mainly formed via 295 the NO₃ oxidation of biogenic VOCs (especially of monoterpenes). In the JULIAC campaign, significant 296 nocturnal oxidized OA production in all seasons is observed, and rich particulate organic nitrate during summer 297 has been found to originate from the NO₃ oxidation of biogenic VOCs in a previous study (Liu et al., 2024). 298 Additionally, a high level of organic nitrate contribution, up to 20% of the submicron nitrate, is observed during 299 wintertime of the JULIAC campaign in Figure 3, which is demonstrated to be related to the NO₃ chemistry of 300 anthropogenic VOCs, such as phenolics from residential heating (Liu et al., 2024). 301 The concentration of organosulfate is the highest in summer (JULIAC-III, up to 2.5 µg/m³) (Figure 3), followed 302 by autumn (JULIAC-IV, up to 0.85 µg/m³). Previous studies have reported that the most abundant aerosol 303 organosulfate species are mainly derived from the oxidation of isoprene and monoterpenes (Wang et al., 2021a). 304 The strong correlation between organosulfate and biogenic OOA during summer (JULIAC-III; see Fig. S3) 305 indicates that biogenic precursors also play a dominant role in the formation of organosulfate during this period. 306 In addition, the high consistency between the variation of biogenic OOA and organosulfate concentrations, as 307 well as the total surface and volume of aerosols detected by SMPS (Table S8), demonstrates that multi-phase 308 reactions involving SOA and sulfur dioxide (SO₂) are one potential pathway for organosulfate formation during 309 summer. A previous chamber experiment on organosulfate formation from multiphase reactions (Yao et al., 310 2019) emphasizes the crucial role of ALWC in regulating the reactive uptake coefficient of SO₂, ultimately 311 influencing aerosol organosulfate formation. In our study, we observed significantly higher organosulfate 312 concentration during a summertime heatwave event. During the heatwave event, despite a modest 10% decrease 313 in RH, the ALWC increased by a factor of 2.3 compared to the summer period before the heatwave. This 314 increase is likely driven by enhanced concentrations of particulate sulfate, nitrate, and organics (Meng et al., 315 2024), which can contribute to greater aerosol hygroscopicity and subsequently promote SO₂ uptake and 316 organosulfate formation. However, due to the absence of SO₂ measurements in this study, this interpretation 317 remains highly uncertain. More investigations of the heatwave event will be discussed in Section 4.2. Figure 3 318 further illustrates that the mass fraction of organosulfate to the total sulfate shows a high relative value of 20-319 31% during cold seasons (autumn and winter) compared to values of 12-16% during warmer seasons (spring 320 and summer). Numerous laboratory studies have demonstrated that organosulfate can be produced through 321 aqueous-phase oxidation of aromatic compounds in the presence of inorganic sulfate (Wang et al., 2021b; 322 Huang et al., 2020). The elevated ALWC and enhanced continuous anthropogenic activities during colder

Figure 3: Seasonal variation in the concentrations of aerosol bulk components (organics, sulfate, nitrate,

seasons, such as residential heating (Section 4.1), may further promote the aqueous-phase formation of organosulfate. However, further research is required to reach a definitive conclusion.

The feasibility of the method used here to calculate organosulfate concentrations (Section 2.3) has been evaluated in a previous study (Schueneman et al., 2021). The results indicate that this method can reliably determine ambient organosulfate concentrations when aerosol properties fall within a specific range: aerosol acidity pH > 0 and an ammonium nitrate fraction below 0.3 (corresponding to condition II, marked by red dashed box in Figure 4). Outside of this range, there is a high likelihood that organosulfate concentrations are underestimated. In this study, high concentrations of aerosol organosulfate were found in summer and autumn based on this method, with high reliability indicated by 84–99% of the periods falling within condition II (Figure 4). In contrast, the greatest uncertainty occurs in winter, when only 43% of the measurements meet condition II, suggesting an underestimation of organosulfate concentrations during that season.

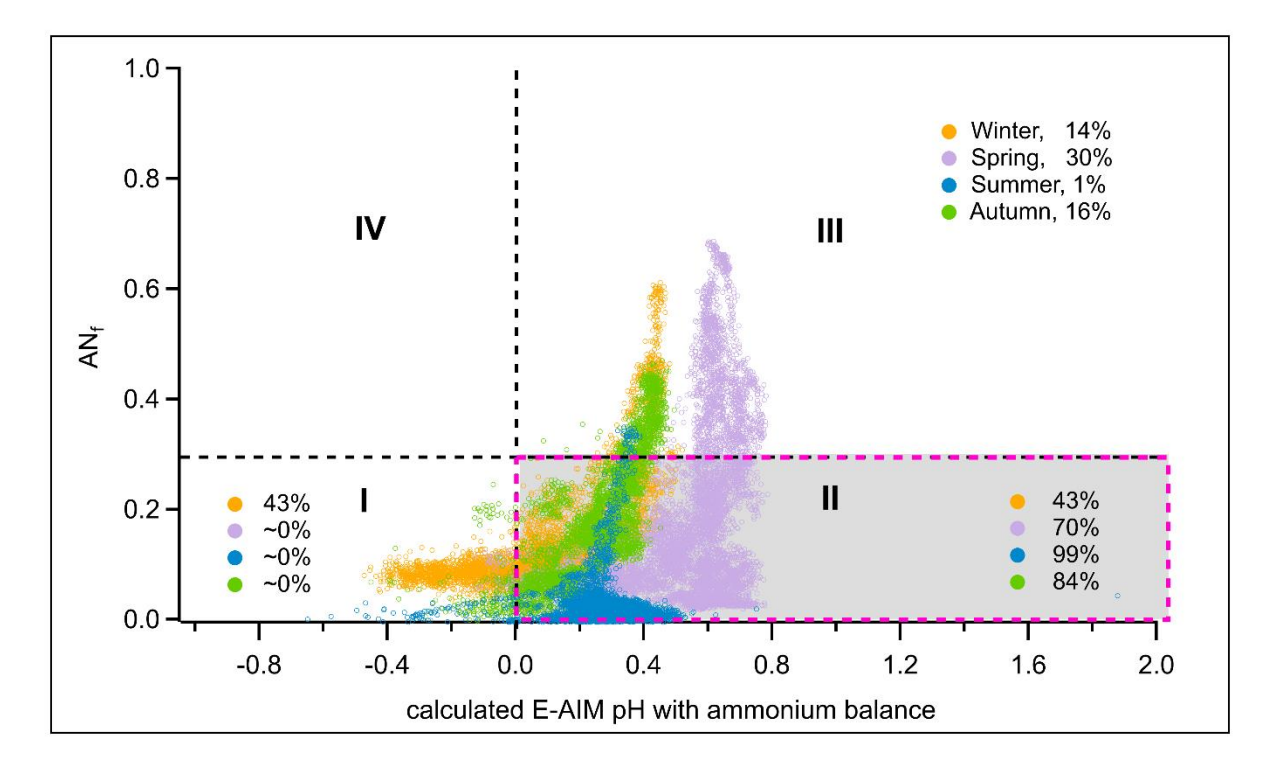


Figure 4: Distribution of aerosol data points measured during the four seasons of the JULIAC campaign for chemical conditions defined by the ammonium nitrate mass fraction (AN_f) and the pH predicted by the Extended Aerosol Inorganics Model (E-AIM) as established by Schueneman et al. (2021). The E-AIM pH was estimated from the measured ammonium balance using HR-ToF-AMS via the empirical calculation method introduced by Schueneman et al. (2021). For all seasons, the fractions of data points under the four conditions were calculated and displayed within the corresponding areas.

4 Discussion

4.1 Overview of seasonal sources of organic aerosols

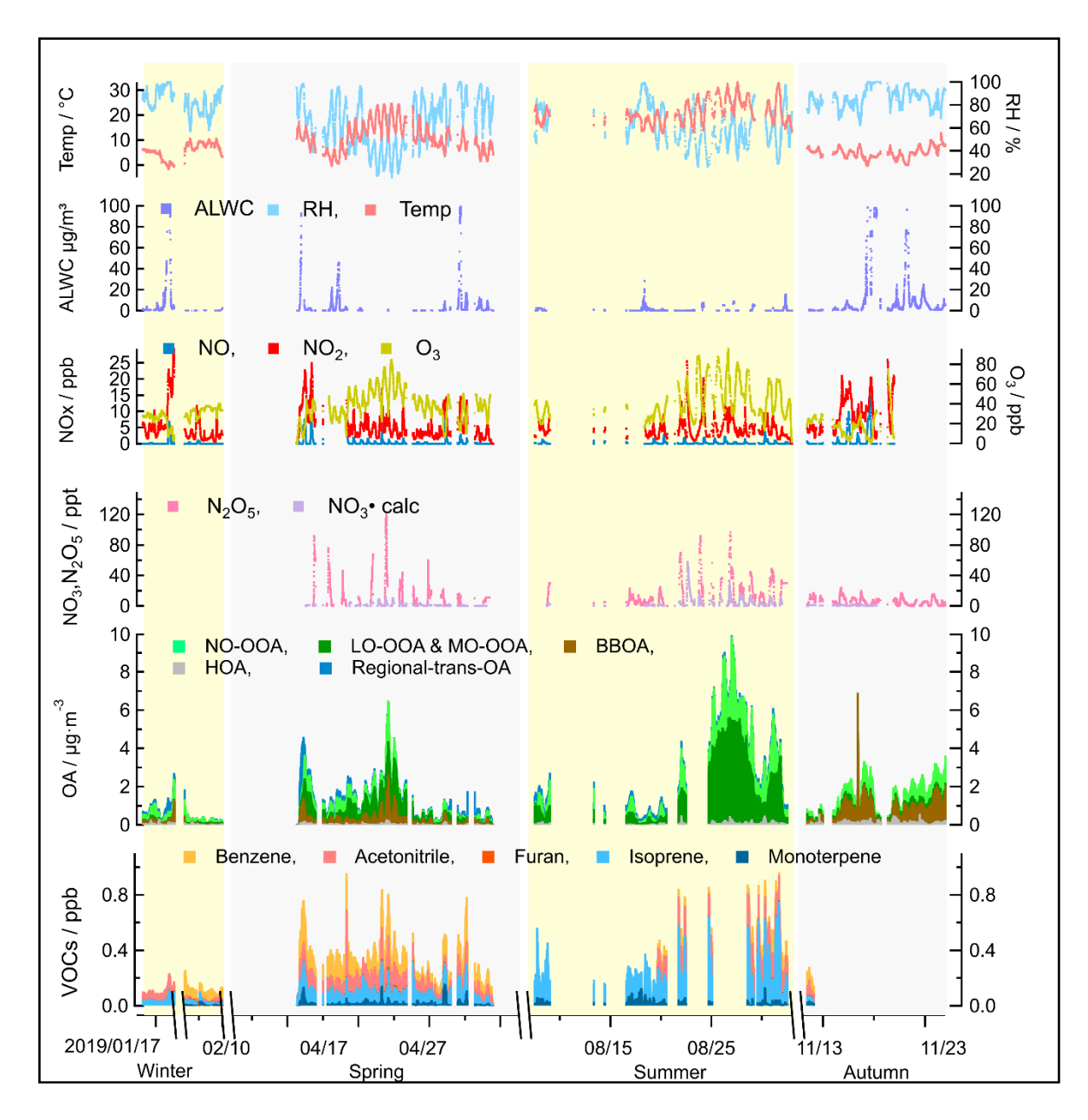


Figure 5: Overview of seasonal variations in source contributions derived from the PMF analysis of OA measurements, including supporting ambient measurements that can be used to identify sources, such as ALWC, trace gase concentrations (VOCs, O₃, NO_x, N₂O₅, NO₃ radicals), and meteorological parameters (temperature and RH), measured during the JULIAC campaign.

The seasonal variations of meteorological parameters (e.g., RH, wind conditions) and various tracers, including VOCs (e.g., monoterpenes, furan), radicals, trace gases (e.g., NO, NO₂, CO), are displayed in Figure 5. For the OA concentrations, the contributions of the identified sources are shown, with the complete mass spectra and diurnal patterns of seasonal OA sources provided in Fig. S4–S7. The comprehensive measurements enhance and strengthen the accuracy of the identification of POA sources and improve the understanding of the dominant mechanisms driving SOA formation (Liu et al., 2024).

Overall, SOA formation, consisting of LO-OOA, MO-OOA, and NO-OOA, dominates the OA mass in most seasons, contributing 46% to 88% of total OA (Figure 5, Figure 6). The only exception was observed in autumn, when primary emissions, particularly from biomass-burning, became more abundant. Nighttime SOA formation via NO₃-initiated oxidation, represented by NO-OOA, accounts for 21% to 48% of the total OA, highlighting the importance of nocturnal oxidation processes (Liu et al., 2024). The balance of daytime (LO-OOA, MO-OOA) and nighttime (NO-OOA) oxidation varies seasonally, reflecting shifts in the dominant OA formation pathways. In summer, daytime biogenic oxidation processes dominate, contributing more than 50% of the OA mass. Conversely, during colder periods such as autumn and winter, nighttime oxidation surpasses daytime oxidation, indicating a stronger influence of nocturnal pathways. POA and SOA related to biomass-burning sources comprise 83% of the total OA mass during autumn. This emphasizes the need for emission control measures targeting biomass-burning, especially with respect to residential heating and industrial activities (Section 4.1.1) to improve air quality in autumn and winter. The seasonal changes of OA source factors are displayed in the space of fCO₂⁺ (fragment fraction of CO₂⁺ in OA) vs fC₂H₃O⁺ (fragment fraction of C₂H₃O⁺ in OA) as shown in Figure 6, complemented by a correlation analysis of the source spectra (Table S3-S5). Primary emissions, represented by hydrocarbon-like OA (HOA) and biomass-burning OA (BBOA), cluster at low fCO2+ and low fC₂H₃O⁺ values, similar to primary source characteristics reported in previous studies (Sun et al., 2012; Zhang et al., 2015; Crippa et al., 2013; Chen et al., 2015). Seasonal variability in biomass-burning emissions is evident from the scattered distribution of BBOA (Section 4.1.1). For secondary sources, LO-OOA factors found during spring and summer have higher fC₂H₃O⁺ but lower fCO₂⁺ than the MO-OOA factors in winter and autumn, which implies biogenic derived SOA formation during spring and summer (Canonaco et al., 2015). For nocturnal oxidation sources, NO-OOA factors cluster closely in the fCO₂+ vs. fC₂H₃O+ space in spring, autumn and winter, while summer NO-OOA exhibits the highest fC₂H₃O⁺ and lowest fCO₂⁺ values. The distinct oxidation level of summer NO-OOA, as discussed in the prior study (Liu et al., 2024), is attributed to biogenic precursors driving NO₃-initiated oxidation in summer, in contrast to biomass-burning emissions being the precursors in the other seasons.

355

356

357

358

359

360

361

362

363

364

365

366

367

368

369

370

371

372

373

374

375

376

377

378

379

380 381

382

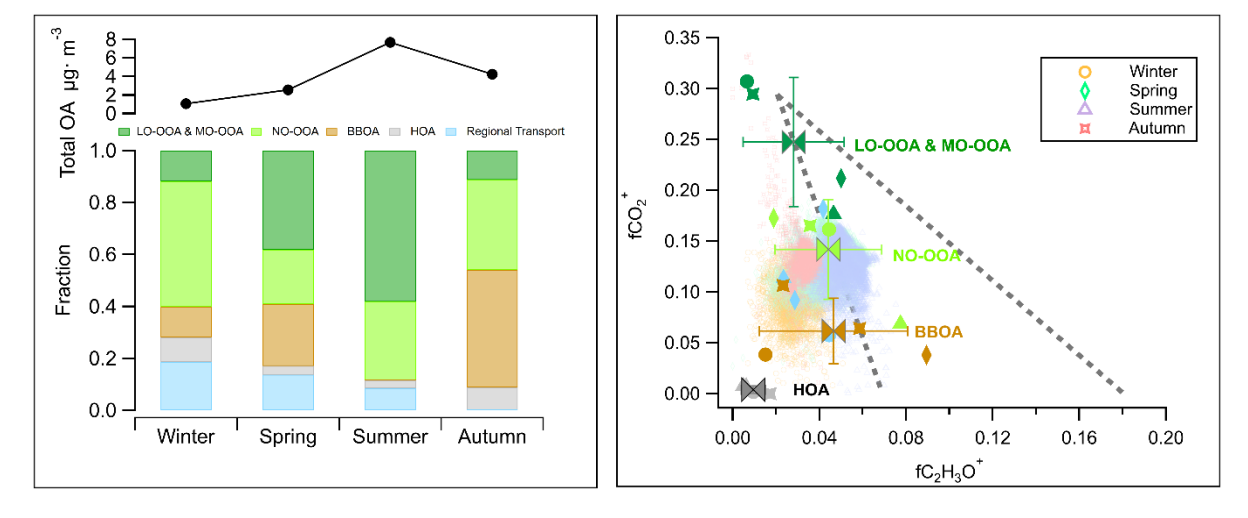
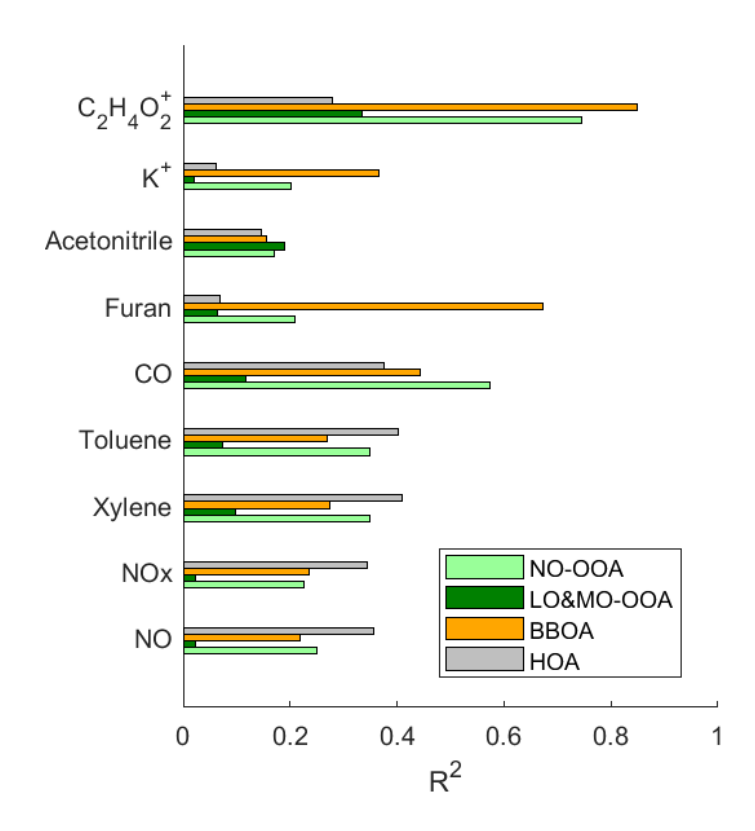


Figure 6: Left panel: Comparison of the average total mass concentration of OA measured by HR-ToF-AMS and the mass fraction of primary and secondary sources' contributions to OA during the JULIAC campaign. Right panel: fCO₂+ (fraction of fragment CO₂+ in OA) vs fC₂H₃O+ (fraction of fragment

 $C_2H_3O^+$ in OA) for all OA during the JULIAC campaign (small transparent dots). The OA source factors (including LO-OOA, MO-OOA, NO-OOA, BBOA, HOA, and regional transport factors) resolved by PMF during each season are shown in fCO_2^+ vs $fC_2H_3O^+$ space (the marker types representing the different seasons, the marker color stands for factor type). Mean values and standard deviations for these four types of source factors are also displayed. The coarser dashed lines represent the f44/f43 distribution triangular region of ambient OOA factors reported in Ng et al. (2010), where f44/f43 corresponds to the mass to charge ratio of CO_2^+ (m/z 44) to $C_2H_3O^+$ (m/z 43).

4.1.1 Primary emissions of organic aerosols

The HOA factors show the lowest O:C ratios (0.03-0.13) and the highest H:C ratios (1.61-2.1) among all source factors identified in the JULIAC campaign (Fig. S4-S7), consistent with previous results (DeCarlo et al., 2010; Mohr et al., 2012; Crippa et al., 2013; Sun et al., 2016). A comparison of the HOA spectra with previous studies is presented in Table S3, showing high correlation coefficients (R^2 ranging from 0.72 to 0.99) and θ , the angular distance between unit mass spectra vectors (Kostenidou et al., 2009), between 12.8° and 33.1°, which confirms the robustness of the method to identify HOA in this study. The diurnal pattern of the HOA factor shows a significant peak during the morning rush hour, indicating that traffic exhaust is the primary source. In Figure 7, the HOA factor shows the highest correlation coefficients with the traffic emission tracer gases compared to other factors, with R^2 values of 0.36 for NO, 0.35 for NO_x, 0.41 for toluene, and 0.40 for xylene. Additionally, the diurnal variations of these traffic emission tracer gases are well correlated with the variation of HOA (Fig. S8), which further supports our conclusion that the HOA source mainly represents the OA contribution from traffic emissions.



toluene), trace gases of combustion and biomass-burning (CO, furan, acetonitrile), and characteristic 406 407 aerosol fragments of biomass-burning (K+, C₂H₄O₂+). OA regional transport factors are not shown due to 408 their extremely low correlation with all primary emission tracers. 409 Characteristic fragments C₂H₄O₂⁺ (m/z 60) and C₃H₅O₂⁺ (m/z 73) are well-established indicators for biomass-410 burning in AMS mass spectra (Simoneit et al., 1999; Alfarra et al., 2007). In this study, these ion mass signals 411 are prominently detected in the BBOA factor spectrum. Furthermore, the BBOA time series aligns closely with 412 the time series of fragment C₂H₄O₂⁺ (m/z 60) during the whole JULIAC campaign, showing the highest 413 correlation coefficient of $R^2 = 0.85$ (Figure 7). In addition, the correlation coefficients between the time series of 414 the OA factors and the biomass-burning tracers, such as furan (Akherati et al., 2020; Coggon et al., 2016) and 415 aerosol potassium (K⁺) (Li et al., 2003; Yu et al., 2018; Zhang et al., 2013; Tao et al., 2014) are shown in Fig. 7. 416 The BBOA factor exhibits a significantly higher correlation value with all mentioned tracers than other primary 417 sources (HOA) and secondary sources (LO-OOA and MO-OOA), supporting its identification as BBOA. The 418 BBOA factors show a lower O:C ratio (0.28 to 0.36) than the OOA factors but a higher ratio than the HOA 419 factors, consistent with previously reported BBOA oxidation levels (Mohr et al., 2012; DeCarlo et al., 2010; 420 Aiken et al., 2009). The high-resolution BBOA spectra from prior studies (Mohr et al., 2012; Hu et al., 2013) 421 are similar to the BBOA spectra from each JULIAC phase (Table S4). The BBOA identified in this study 422 closely resembles findings from Hu et al. (2013), with R² ranging from 0.76 to 0.94 and θ from 14.2° to 27.9°, 423 confirming the BBOA factor identification. 424 As mentioned above, BBOA source factors show seasonal differences (Figure 6), suggesting distinct types of biomass-burning during each season. The BBOA factor observed in spring is also associated with a different 425 426 type of biomass-burning, as indicated by the high fC₂H₃O⁺ ratio (Fig. 6). This BBOA factor is confirmed to be 427 related to the regional transport of wildfire emissions (Section 4.1.3.2). The most abundant OA contribution 428 from biomass-burning is found in autumn, where two distinct BBOA sources are identified: one dominated by 429 local emissions and the other associated with regional transport (Fig. S2). The local BBOA source is likely 430 related to residential heating and nearby emissions from the sugar factory, which have active production of 431 sugar only during the autumn phase. Some industries in Germany, such as sugar factories, are adopting biomass 432 fuels like beet pulp to reduce fossil fuel use and achieve climate-neutral production by 2040 (Insight, 2023). 433 This shift is part of a broader energy transition that includes biomass-burning as an alternative energy source 434 (Lipiäinen et al., 2022; Bataille, 2020). These changes are expected to affect anthropogenic emissions and, in 435 turn, atmospheric chemistry. 436 4.1.2 Secondary formation of organic aerosols 437 In this study, LO-OOA is predominantly observed during spring and summer, while MO-OOA is dominant 438 during autumn and winter (Fig. S4-S7). Both LO-OOA and MO-OOA spectra exhibited strong contributions 439 from fragments at m/z 44 (with the signal at m/z 28 assumed to be equal to that at m/z 44 (Aiken et al., 2008)), 440 with dominant ion families $C_x H_y O$ and $C_x H_y O_z$ (z > 1). The oxidation degrees of LO-OOA and MO-OOA are 441 the highest among OA sources in all seasons, with O:C ratios ranging from 0.7 to 1.0, comparable to previous 442 studies (Hu et al., 2013; Xu et al., 2015c; Sun et al., 2016; Dai et al., 2019). The high-resolution mass spectra of

Figure 7: Cross-correlation R² of major OA sources among tracer gases of car exhaust (NO, NO_x, xylene,

443 LO-OOA and MO-OOA identified in this study can be compared with those of prior source apportionment 444 studies (Mohr et al., 2012; Crippa et al., 2013; Hayes et al., 2013; Hu et al., 2013; Hu et al., 2015), with R² 0.93 445 - 0.99 and θ ranging from 5.9° to 15.7°. The highest similarity is observed with the results of Hu et al. (2013). 446 LO-OOA and MO-OOA are the only source factors showing distinct diurnal peaks around noon (UTC 11:00-447 14:00, Fig. S4-S7), a pattern characteristic of SOA formed through photochemical processes. High correlations 448 between O₃ and LO-OOA or MO-OOA time series are observed during the warmer seasons, specifically in 449 spring and summer, with R² values of 0.56 and 0.71, respectively. Therefore, the LO-OOA and MO-OOA 450 factors identified during the JULIAC campaign are mainly dominated by daytime oxidation processes. 451 The NO-OOA factor resolved in this study is attributed to nocturnal OOA formation dominated by NO₃ 452 chemistry, with a diurnal peak around midnight (UTC 20:00-04:00, Fig. S4-S7). The O:C ratios of NO-OOA 453 vary from 0.39 to 0.91, which depends on the seasonal precursors, biogenic VOCs, particularly monoterpenes in 454 summer, and biomass-burning emissions in the colder seasons (Liu et al., 2024). The potential phase 455 partitioning, nocturnal boundary layer development, and various reaction pathways (such as ozonolysis, aqueous 456 phase reactions, and NO₃ chemistry) have been thoroughly discussed in the study of Liu et al. (2024). That study 457 has introduced an improved source apportionment method, using PMF analysis of aerosol organic and nitrate 458 bulk measurements to differentiate between the OOA formed from nocturnal and daytime oxidation. Also, the 459 NO-OOA factor shows typical characteristics, such as a higher ion intensity fraction of nitrate fragments 460 $(NO^++NO_2^+)$ normalized to the total ion intensity $(f(NO^++NO_2^+)>0.1)$ and higher nitrogen to carbon ratios 461 (N:C, 0.05-0.15) than the OOA formed from daytime oxidation (LO-OOA and MO-OOA). High OA mass 462 fractions of NO-OOA (21%-48%) highlight a significant formation via NO₃-initiated nocturnal oxidation in all 463 seasons. 464 Overall, SOA sources, represented by OOA factors (LO-OOA, MO-OOA, NO-OOA), contribute 46%-88% of 465 the total OA mass throughout the campaign. Seasonal variations in the relative contributions of daytime (LO-466 OOA, MO-OOA) and nighttime (NO-OOA) oxidation pathways indicate that OOA formation is dominated by 467 daytime oxidation of biogenic VOCs in spring and summer, accounting for 64-66% of OOA. In contrast, during autumn and winter, nocturnal oxidation (NO-OOA) exceeds daytime oxidation and dominates OOA formation, 468 contributing 75-80%. 469 470 Regional transport effect on organic aerosols 4.1.3 471 In this study, OA transport events are identified by a PMF analysis. These events are air masses originating from 472 marine regions or wildfires. The regional influences inferred from source factor characteristics align well with 473 trajectory model results, further supporting the PMF analysis as an appropriate method for resolving regional 474 transport events. However, the PMF analysis becomes less effective under conditions of persistent and strong 475 regional influence. For instance, during autumn, sustained strong winds can create a continuous influx of 476 regional air masses, leading to a more homogeneous aerosol composition. This continuity reduces the variability

needed for PMF to distinguish between distinct sources or transport patterns. Additional discussion on the

477

478

regional transport of OA is provided below.

4.1.3.1 Regional transport from the ocean

The OA contribution from regional transport of the ocean is attributed during spring (JULIAC-II) and summer (JULIAC-III) to the MSA-OA source factor. As shown in Figure 8, the MSA-OA factor contains typical marker fragments: CHS⁺(m/z 44.98), CH₂SO₂⁺(m/z 77.98), CH₃SO₂⁺(m/z 78.99), and CH₄SO₃⁺(m/z 95.99). Among these fragments, CH₃SO₂⁺ is regarded to be a characteristic fragment for the MSA containing ambient aerosols and has been reported as the most abundant organosulfate ion in the MSA-OA factor profile in previous studies (Zorn et al., 2008; Huang et al., 2017). The MSA-OA factor in this study shows a high similarity in the marker fragments as well as in the full mass spectrum (R²=0.84) with the MSA-OA factor resolved by Schlag et al. (2017). We also find the ion fragment CH₃S⁺ (m/z 47.00) in the MSA-OA factor, which has been mentioned in Schmale et al. (2013). The low intensity of the CH₃S⁺ (m/z 47.00) ion mass signal may be one possible reason why it has not been reported frequently so far and is not commonly considered a stable marker ion.

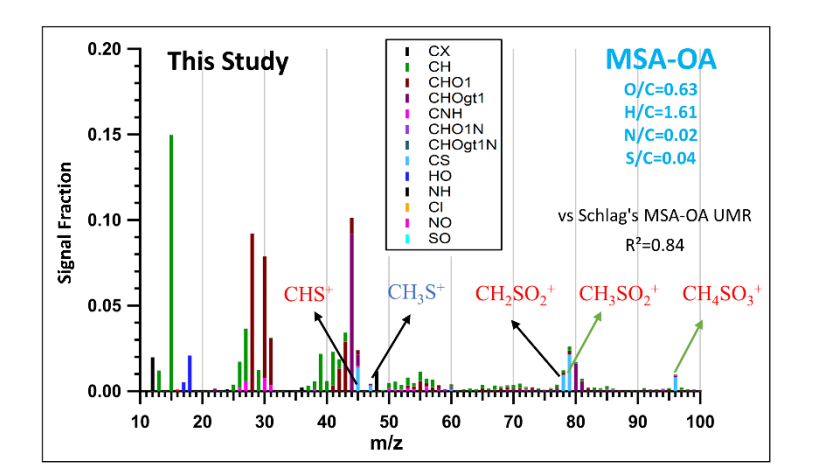


Figure 8: MSA-OA factor profile of this study. Typical MSA marker fragments: CHS^+ (m/z 44.98), CH_3S^+ (m/z 47.00), $CH_2SO_2^+$ (m/z 77.98), $CH_3SO_2^+$ (m/z 78.99), and $CH_4SO_3^+$ (m/z 95.99) are highlighted in the factor profile. Normalized ion attribution is colored by corresponding ion family groups, and elemental ratios (O/C, H/C, N/C, S/C) of the MSA-OA factor are also marked in the graph. The y-axis presents the ion signal intensity fraction.

In Figure 9 c), 24-hour back-trajectories (yellow) show a fast air mass transport from ocean to the measurement site, which occurred 21% of the time during spring (JULIAC-II). During this time, the concentration of the MSA-OA factor increases while the contributions of other sources remain low and stable. The polar diagram in Figure 9 d) shows that high MSA-OA concentrations (>0.1 μg/m³) are associated with high wind speeds (>10 m/s) originating from the northwest, which align well with the marine origin trajectory. Additionally, the time series of the aerosol MSA is calculated using two different characteristic ion methodologies (Ge et al., 2012; Huang et al., 2015) (Figure 9 b), which also shows good agreement with the variations of MSA-OA factor, with a correlation coefficient R²=0.95 for MSA-OA vs MSA (Ge method, (Ge et al., 2012) and 0.94 for MSA-OA vs MSA (HKUST method, (Huang et al., 2015)). Because the MSA-OA factor is not only composed of MSA but also contains other organic fragments, the concentration level of the MSA-OA factor is around 3 times higher than the concentration of the aerosol MSA. Overall, this comparison supports the influence of marine transport at this inland site.

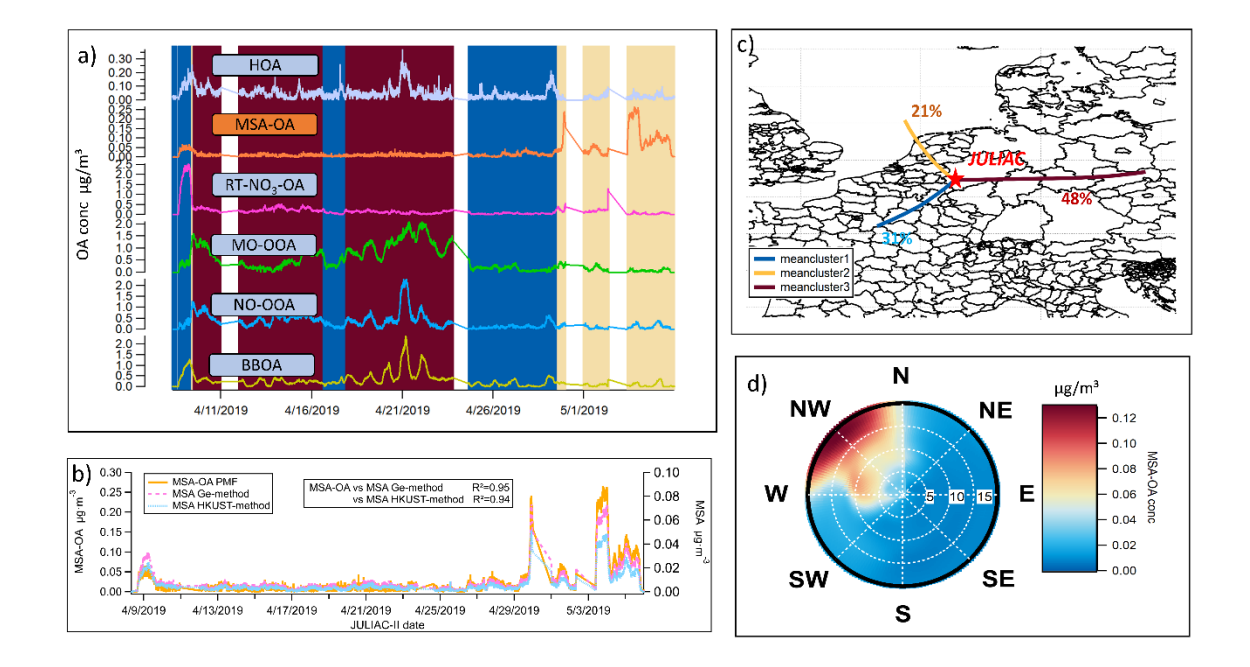


Figure 9: a) Time series of all source factors of OA resolved by the PMF analysis during spring (JULIAC-II) with the background color corresponding to different clusters of the 24-hour back-trajectories (of panel c); b) Comparison of MSA variations calculated using the Ge method (Ge et al., 2012) and the HKUST method (Huang et al., 2015), and the contribution variation of MSA-OA source resolved by PMF during spring (JULIAC-II). c) Clusters of 24-hour back-trajectories simulated by HYSPLIT4 during spring (JULIAC-II) at the Jülich site, with the proportion of each trajectory cluster marked. d) Polar diagram of MSA-OA concentration during spring, based on non-parametric wind regressions. The wind speeds are shown as the radius with the unit of m/s.

In contrast, during summer (JULIAC-III), the contribution of the MSA-OA factor and the calculated concentration of MSA (using the Ge and HKUST methods) both increase during periods when air masses are not transported from ocean (Figure 10a). The corresponding 72-hour back trajectory cluster (Figure 10c) shows a slow movement of air masses or relatively steady conditions of the local atmosphere in summer, suggesting that local emissions are the dominant influence at the site during this period. Additionally, poor agreement of the time series in calculated MSA and MSA-OA factors is also shown, with an R² value of approximately 0.2. The strong local formation of organosulfate during summer (Figure 3) may complicate the identification of MSA and potentially introduce a bias. Another possibility is the existence of unidentified terrestrial sources for aerosol MSA formation, as suggested by previous studies (Zhou et al., 2017; Young et al., 2016; Ge et al., 2012), though the mechanisms remain unclear and warrant further investigation. However, using the mass fraction of MSA-OA normalized to the total OA and the mass fraction of MSA normalized to the total aerosol leads to notable differences in the results. In Figure 10 b, the variations in MSA-OA and MSA mass fractions show an increasing trend in their similarity (R² = 0.72–0.76) and exhibit better agreement with the back trajectory analysis. In conclusion, the observed increase in the MSA-OA concentration during the non-marine-transported period in summer could be attributed to a methodological bias or a potential unknown formation pathway of

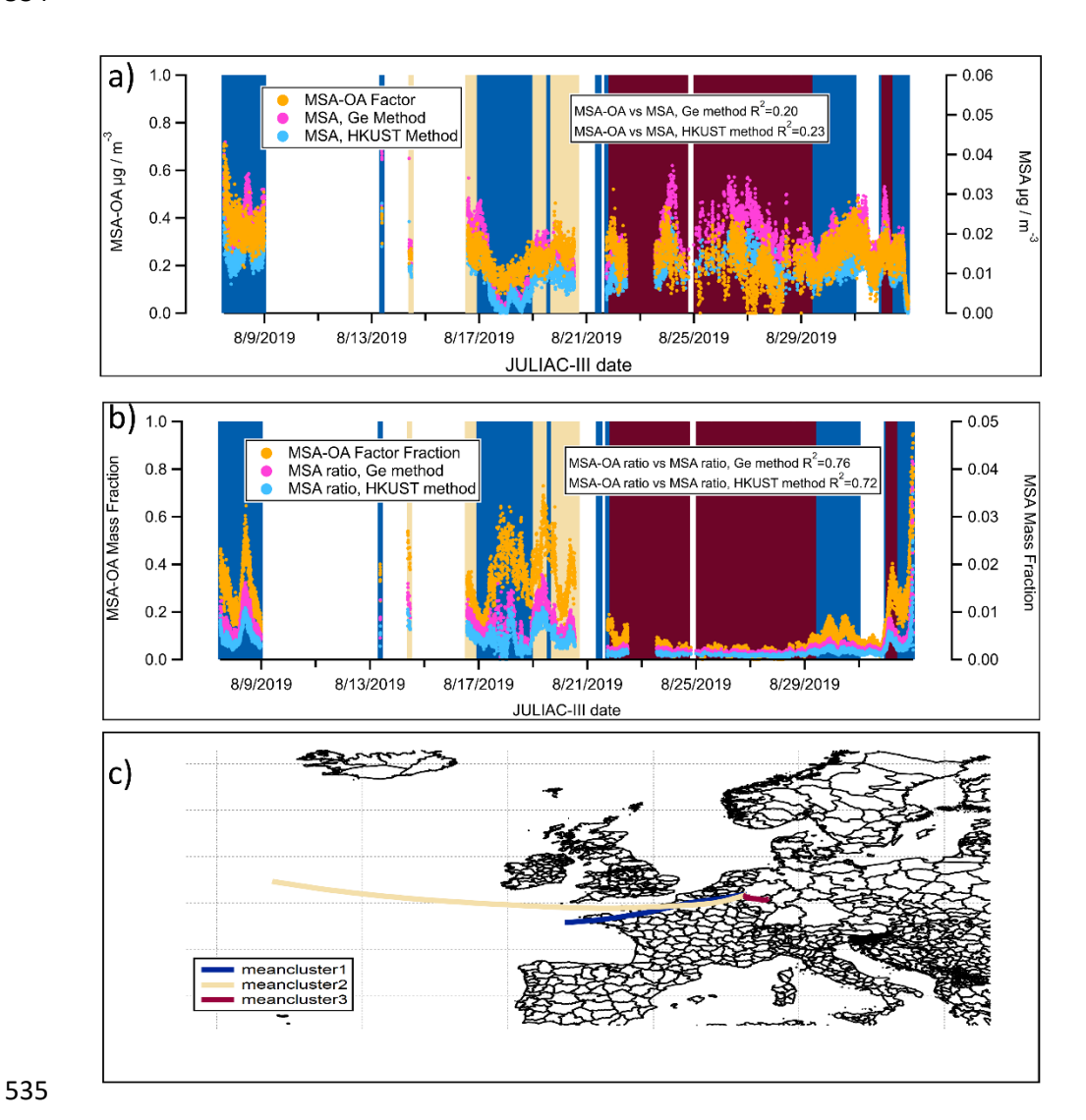


Figure 10: a) Time series of the contribution of the MSA-OA factor and the concentrations of calculated MSA using the Ge and HKUST methods during the summer (JULIAC-III), with background colors matching the corresponding back-trajectory clusters; b) Mass fraction of the MSA-OA factor (normalized to the aerosol organic mass) and MSA (normalized to the total aerosol mass) calculated using the Ge and HKUST methods during the summer (JULIAC-III); c) Clusters of 72-hour back-trajectories during the summer (JULIAC-III), simulated by HYSPLIT4.

${\bf 4.1.3.2} \qquad {\bf Regional\ transport\ of\ wild fire\ plumes\ from\ the\ Russian\ area}$

A regional transport event of wildfire plumes during spring is confirmed using source apportionment analysis coupled with the analysis of 72-h back trajectories (an extension of the previous 24-h back trajectory) and the hotspot data from MODIS (Aqua & Terra) with a resolution of 1 km and VIIRS (S-NPP, NOAA-20 & NOAA-21) with a resolution of 375 m, provided by the Fire Information for Resource Management System (FIRMS) of NASA (Figure 11). Hotspots are detected based on thermal anomalies in satellite imagery, and therefore single

and isolated dots are often due to noise but not real fire. Wildfire activity indicated by clusteres of hotspot are observed during spring in the Russian region and affects this study area via long-distance transport. During this time, BBOA concentrations peak in spring. In addition, the mass fraction of the biomass-burning tracer, fC₂H₄O₂+, in BBOA from spring is clearly lower than that observed in other seasons (Fig. S9). This observation is consistent with chamber experiments of biomass-burning dark aging, where fC₂H₄O₂+ decreases with increasing aging time (Kodros et al., 2020). This further confirms that the BBOA in spring is primarily influenced by the regional transport of fire emissions. The high frequency of fires in Russia during spring is consistent with the results of previous studies on the occurrence of Russian wildfires (Kharuk and Ponomarev, 2017). As discussed previously (Liu et al., 2024), the NO-OOA formation during spring is predominantly driven by nitrate radical (NO₃) chemistry of biomass-burning emissions. Consequently, the POA and SOA linked to the regional transport of wildfire plumes contribute to approximately half of the total OA observed during spring. This highlights wildfire emissions transport as a key factor influencing the atmospheric conditions at the site during spring.

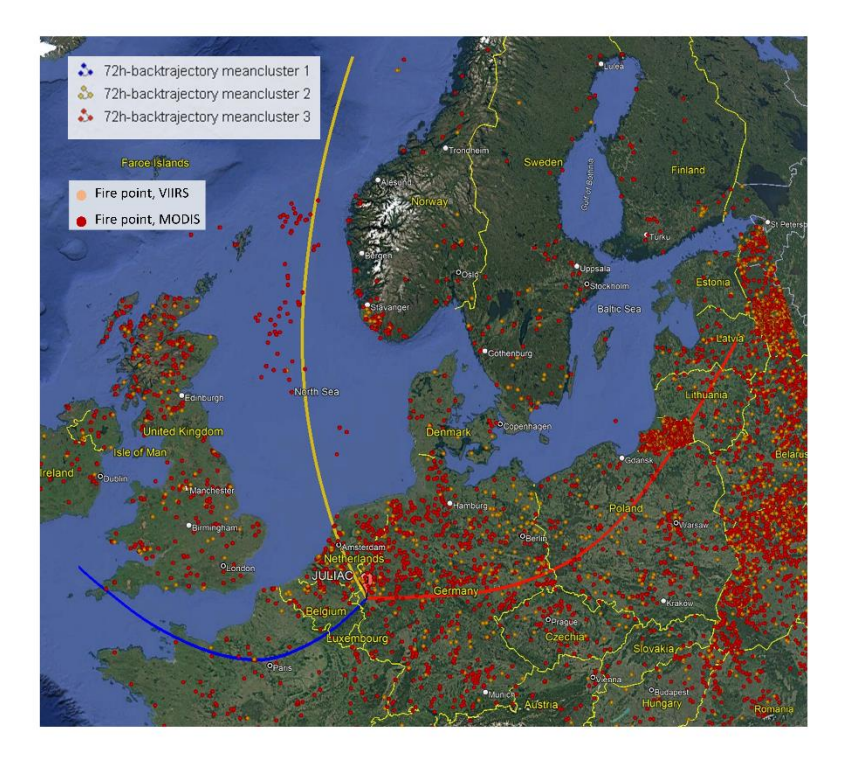


Figure 11: Trajectory clusters (yellow, blue, and red lines) of the 72-hour back-trajectories simulated by HYSPLIT4 at the measurement site in Jülich during spring (JULIAC-II). Hotspot counts during spring are shown as yellow (VIIRS) and red (MODIS) dots, provided by the Fire Information for Resource Management System (FIRMS) of NASA (accessible at https://firms.modaps.eosdis.nasa.gov/). Map background © Google Earth, image © 2025 Maxar Technologies.

4.1.3.3 Seasonal variability of regional contributions to aerosols

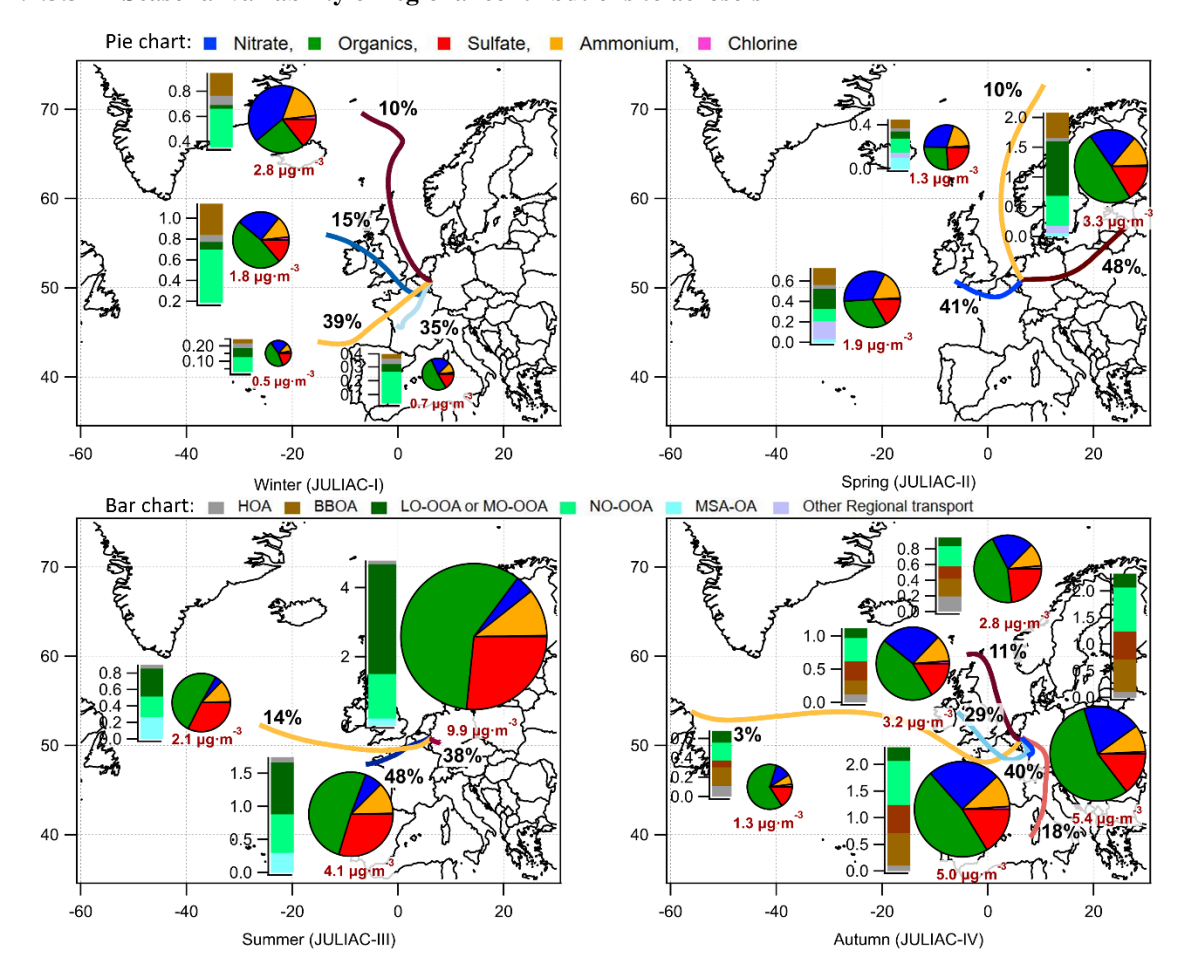


Figure 12: Trajectory clusters representing 72-hour back-trajectories simulated by HYSPLIT4 for each season at the Jülich site, annotated with the frequency proportions of each respective cluster.

Additionally, the average composition and concentration of submicron aerosols, together with the average source contributions of organics derived from PMF analysis, are presented for each corresponding cluster period.

To further understand the effect of long-range transport on the aerosol composition at the site, the back-trajectory clusters combined with the average aerosol composition and source contributions of organics during the corresponding cluster periods are analyzed. As shown in Figure 12, more than half of the long-range transport plumes originate from the west of the site. During the periods influenced by transport from these directions, the total aerosol mass consistently shows a clear decrease compared to the periods dominated by local emissions in each season, implying a general cleansing effect for the aerosol level at the site by regional transport. The only exception occurred in winter (JULIAC-I), when the aerosol mass reaches a maximum due to regional influences from air masses originating in the northwest, with an enhanced mass fraction of nitrate and an increased BBOA contribution. A clear increase in the contributions of sulfate is also observed when trajectories originate from marine regions. This increase is accompanied by a rise in the MSA-OA fraction, which is associated with the enhanced activity of phytoplankton and anaerobic bacteria in the ocean during summer, the primary natural sources of sulfur-containing compounds (Charlson et al., 1987). A similar increase in sulfate and MSA-OA is observed during spring for marine-origin transport but is absent in colder seasons.

This suggests that the seasonal activity of phytoplankton and anaerobic bacteria plays a significant role in modulating the influence of marine regional transport. In conclusion, regional influences are highly diverse, affected not only by the source regions but also by the seasonal variations in biogenic and anthropogenic activity within these regions.

4.2 Heatwave-induced changes in the formation of OOA

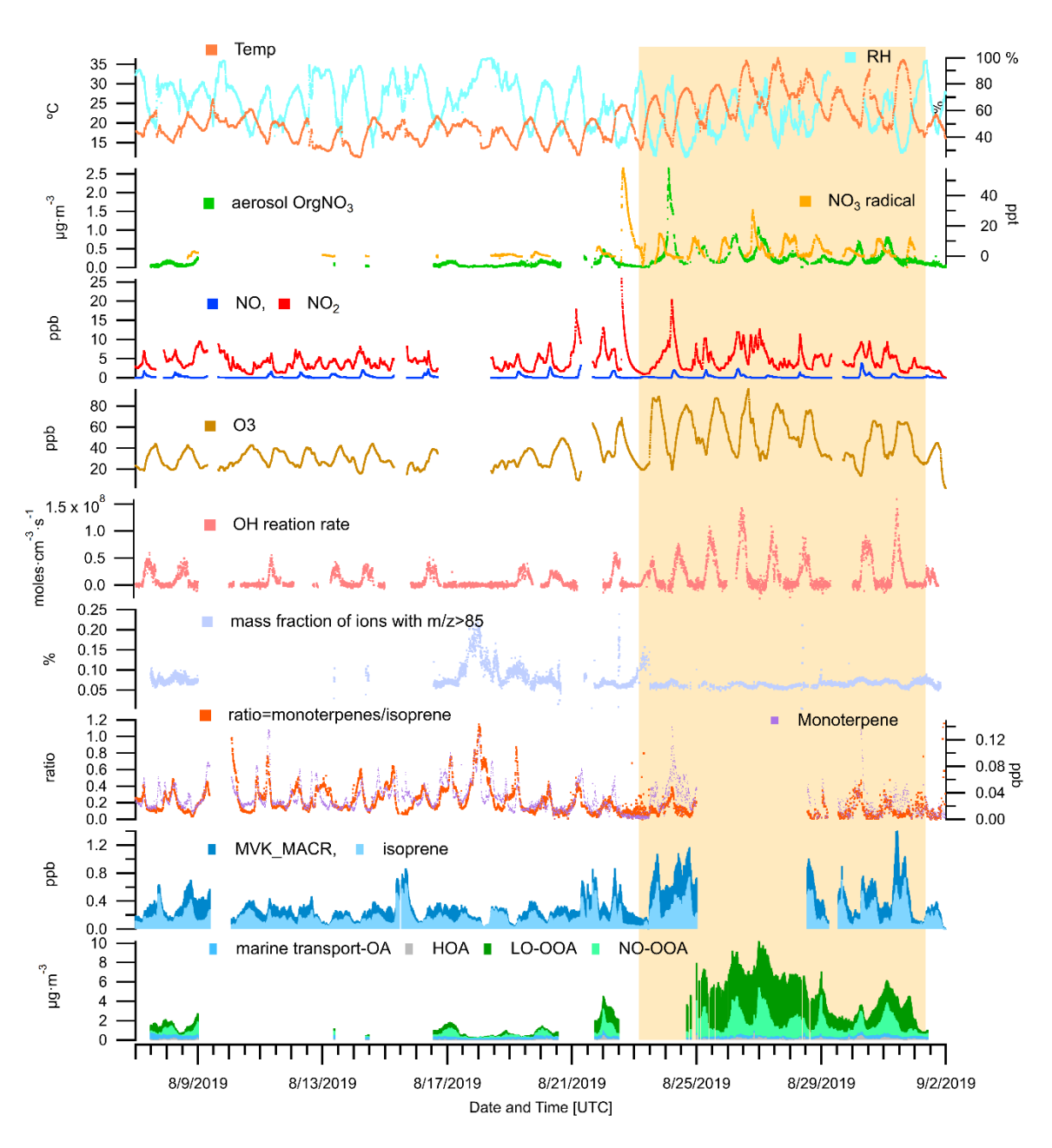


Figure 13: An overview of OA source contributions, ambient measurements of trace gases (VOCs, O₃, NO_x, N₂O₅, NO₃ radicals), meteorological parameters (temperature and RH), and calculated parameters are provided for the JULIAC summer period. The calculated parameters include the OH reaction rate

597 OA measured by the ToF-AMS, and the concentration ratio of monoterpenes to isoprene. The period of 598 the heatwave event observed in summer is highlighted with a yellow background. 599 A previous chamber study (Mentel et al., 2013) has demonstrated that heat and drought stress can reduce 600 monoterpenes emissions, thereby suppressing biogenic OOA formation. In this study, a decrease in 601 monoterpene concentrations is observed during a heatwave event, with the average levels dropping to 60% of 602 the pre-heatwave values (Figure 13). Conversely, isoprene concentration increases by a factor of 1.4, leading to 603 a substantial shift in the monoterpene-to-isoprene concentration ratio, which decreases from 0.24 to 0.11 during 604 the heatwave event. Despite the reduced monoterpene concentrations, no suppression of biogenic OOA 605 formation is observed. On the contrary, total biogenic OOA mass increases notably during the heatwave, with 606 the contribution of LO-OOA rising by a factor of 5 and NO-OOA by a factor of 3. This suggests that, beyond 607 changes in biogenic emissions, other atmospheric processes induced by the heatwave conditions play a critical 608 role in enhancing the OOA formation. 609 The increase of the atmospheric oxidation potential during heatwave events, triggered by elevated temperatures, 610 low RH, and intense radiation, has been reported in previous studies (Desai et al., 2024; Zhang et al., 2024). 611 This phenomenon is primarily reflected in the rise of the concentration of oxidants and the reaction rate of 612 BVOCs. In this study, a similar rise in atmospheric oxidation capacity is suggested by the observed increases in 613 O₃ and NO₃ concentrations, as well as the total reaction rate of OH (Cho et al., 2023), as shown in Figure 13. 614 Consequently, the enhanced formation of OOA from both daytime (LO-OOA) and nighttime (NO-OOA) 615 chemistry may be linked to this increased atmospheric oxidation potential. Additionally, the observed decrease 616 in monoterpene concentrations could be partially attributed to their faster oxidation in the presence of high 617 oxidant levels. 618 In addition, the changes in OA properties during the heatwave event are examined to assess whether shifts in the 619 dominant SOA formation pathways occurred. Figure 14 compares the average OA composition before and during the heatwave, revealing a noticeable decrease in the fraction of ions with m/z > 85 relative to total ions 620 621 during the heatwave. This decline occurs sharply at the onset of the heatwave event, as shown in Fig. 13. 622 Additionally, although the fraction of CO2+ ions increases during the heatwave, the average O/C ratio of OA 623 remains relatively stable (0.57 before and 0.59 during the heatwave). This suggests that the shift of OA 624 composition is not driven by the increased fragmentation of highly oxygenated OA. Previous studies have used 625 the fraction of ions with m/z > 85 as an indicator for the abundance of oligomers in SOA (Faust et al., 2017; 626 Liggio and Li, 2006; Riva et al., 2019). The rapid formation of highly oxygenated organic molecules (HOM) 627 from the oxidation of BVOCs, primarily monoterpenes, is a well-known pathway for biogenic SOA formation 628 (Bianchi et al., 2019). In addition, isoprene has been reported to suppress HOM formation and subsequent SOA 629 production by OH scavenging (McFiggans et al., 2019). However, in this study, a co-increase of isoprene and 630 OOA is observed during the heatwave. As shown in Fig. 14, the isoprene-derived SOA tracer ion, C₅H₆O⁺ (m/z 631 82) (Hu et al., 2015), increases in the OA during the heatwave event, with the mass fraction varying from 1.7% 632 to 4‰ (Fig. S10). When source apportionment is conducted separately for the periods before and during the 633 heatwave, the increase in C₅H₆O⁺ (m/z 82) within LO-OOA is more pronounced (Fig. S11). These findings 634 suggest a potential shift in the SOA formation pathways during the heatwave, where isoprene may play a role in

(derived from measured OH concentrations and OH reactivity), the mass fraction of ions with m/z > 85 in

the aerosol formation and growth. Additionally, particulate organic nitrates and organosulfates both reach their annual maximum during the heatwave period (Figure 3). These findings highlight the need for further investigations of the atmospheric chemistry during heatwaves. A combination of gas- and aerosol-phase molecular measurements could provide new insights into the potential impacts of extreme heat events on SOA formation in the ambient atmosphere.

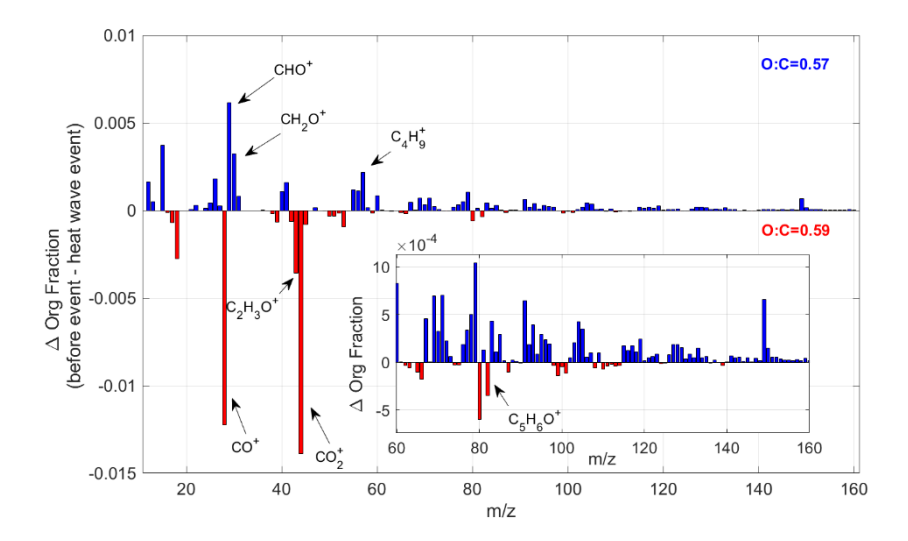


Figure 14: The change in the average organic signal mass fraction, normalized to total OA mass, between pre-heatwave and heatwave periods. The insert window shows the detailed mass spectrum difference at regions of higher molecular weight with m/z>60. The blue color bar shows the ion peaks, which have a higher intensity before the heatwave event, while the red color bar represents the ions enhanced during the heatwave event.

5 Conclusion

The 2019 Jülich Atmospheric Chemistry Project (JULIAC) campaign conducted continuous measurements of submicron aerosol composition, trace gases, and atmospheric conditions at a rural site in Germany during four seasons. Ambient air was sampled from a height of 50 m into the SAPHIR atmospheric simulation chamber, ensuring that all connected instruments sampled the same air and minimizing influence from local emissions. This study indicates that OA dominated the submicron aerosol composition throughout the year, comprising 39%-58% of the aerosol mass, followed by sulfate (16%-26%) and nitrate (5%-26%). Peak organic nitrate concentrations occur in summer, contributing up to 62% of the bulk nitrate, driven by nocturnal NO₃ oxidation. Organosulfates reach their maximum concentrations in summer, likely driven by biogenic formation pathways. Interestingly, organosulfate also contributes significantly to the bulk aerosol sulfate (20% -31%) during winter and autumn, though their source remains uncertain and requires further investigation.

As the major compound of submicron aerosol, OA shows distinct seasonal variations in both mass and chemical properties. The highest OA concentrations with the lowest oxidation levels occur during summer. In contrast, autumn and winter exhibit lower OA concentrations but higher oxidation degrees, with a more pronounced

nocturnal increase in OA concentration. Seasonal source apportionment analysis reveals that over 80% of OA mass originates from SOA formed via both daytime and nighttime oxidation of biogenic emissions during summer. In contrast, OA is dominated by biomass-burning sources during autumn and winter, with POA and related SOA formation of biomass-burning sources contributing 60% to 83% of OA mass. Traffic emissions are found to be a minor OA source throughout the year (3%-10%). These findings suggest that effective air quality mitigation during the cold season should focus on controlling biomass-burning emissions, such as those from residential heating and industrial activities. In addition, the enhancement of SOA formation during the heatwave is attributed to increased atmospheric oxidation potential, driven by elevated oxidant levels (O₃, NO₃, and OH). A shift in SOA formation pathways during the heatwave, potentially influenced by isoprene chemistry, is also observed. These findings highlight the need for further investigation into heatwave-induced changes in atmospheric composition, particularly using molecular-level measurements.

This study examines the seasonal influence of regional transport on aerosol composition. While summer aerosol composition is primarily driven by local emissions and biogenic SOA formation, regional transport significantly influences the colder seasons. OA mass contributions from regional transport sources (marine, wildfire) resolved by source apportionment align well with back trajectory model results, suggesting that source apportionment is a more robust framework than traditional tracer-based methods for interpreting regional influences. Overall, the influence of regional transport at this site generally led to a decrease in total aerosol concentration, except in winter. Notably, identical regional transport pathways exhibit distinct seasonal impacts. For instance, marine plumes contribute clearly to OA only in warmer seasons, driven by enhanced phytoplankton and anaerobic bacterial activity.

Code and data availability

- The data used in this study are available from the Jülich DATA platform (https://doi.org/10.26165/JUELICH-
- 683 DATA/TPPXNL).

Author Contributions

- AH designed the JULIAC campaign and coordinated its execution together with TH, HF, and FH. LL conducted
- the aerosol measurements, performed data analysis, and drafted the manuscript. All co-authors contributed to
- data processing and provided valuable input through extensive discussions during the manuscript preparation.

Competing interests

At least one of the (co-)authors is a member of the editorial board of Atmospheric Chemistry and Physics.

Acknowledgement

- We gratefully thank all JULIAC team members for their valuable discussions and technical and logistical
- support. We also acknowledge the use of AI-assisted tools for language polishing in preparing this manuscript.

694 References

- Aiken, A. C., DeCarlo, P. F., and Jimenez, J. L.: Elemental Analysis of Organic Species with Electron
- 696 Ionization High-Resolution Mass Spectrometry, Analytical Chemistry, 79, 8350-8358,
- 697 https://doi.org/10.1021/ac071150w, 2007.
- 698 Aiken, A. C., DeCarlo, P. F., Kroll, J. H., Worsnop, D. R., Huffman, J. A., Docherty, K. S., Jimenez, J. L.:
- 699 O/C and OM/OC Ratios of Primary, Secondary, and Ambient Organic Aerosols with High-Resolution
- 700 Time-of-Flight Aerosol Mass Spectrometry, Environ Sci Technol, 42, 4478-4485,
- 701 https://doi.org/10.1021/es703009q, 2008.
- 702 Aiken, A. C., Salcedo, D., Cubison, M. J., Huffman, J. A., DeCarlo, P. F., Ulbrich, I. M., Jimenez, J. L.:
- 703 Mexico City aerosol analysis during MILAGRO using high resolution aerosol mass spectrometry at the
- urban supersite (T0) Part 1: Fine particle composition and organic source apportionment, Atmos.
- 705 Chem. Phys., 9, 6633-6653, https://doi.org/10.5194/acp-9-6633-2009, 2009.
- 706 Akherati, A., He, Y., Coggon, M. M., Koss, A. R., Hodshire, A. L., Sekimoto, K., Jathar, S. H.: Oxygenated
- 707 Aromatic Compounds are Important Precursors of Secondary Organic Aerosol in Biomass-Burning
- 708 Emissions, Environ Sci Technol, 54, 8568-8579, https://doi.org/10.1021/acs.est.0c01345, 2020.
- 709 Alfarra, M. R., Prevot, A. S. H., Szidat, S., Sandradewi, J., Weimer, S., Lanz, V. A., Baltensperger, U.:
- 710 Identification of the Mass Spectral Signature of Organic Aerosols from Wood Burning Emissions,
- 711 Environ Sci Technol, 41, 5770-5777, https://doi.org/10.1021/es062289b, 2007.
- 712 Bataille, C.: Low and zero emissions in the steel and cement industries: Barriers, technologies and
- 713 policies, OECD Publishing, 2020.
- Bianchi, F., Kurten, T., Riva, M., Mohr, C., Rissanen, M. P., Roldin, P., Ehn, M.: Highly Oxygenated
- 715 Organic Molecules (HOM) from Gas-Phase Autoxidation Involving Peroxy Radicals: A Key Contributor
- to Atmospheric Aerosol, Chem Rev, 119, 3472-3509, https://doi.org/10.1021/acs.chemrev.8b00395,
- 717 2019.
- Bohn, B. and Zilken, H.: Model-aided radiometric determination of photolysis frequencies in a sunlit
- atmosphere simulation chamber, Atmos. Chem. Phys., 5, 191-206, https://doi.org/10.5194/acp-5-
- 720 <u>191-2005</u>, 2005.
- Bohn, B., Rohrer, F., Brauers, T., and Wahner, A.: Actinometric measurements of NO₂ photolysis
- frequencies in the atmosphere simulation chamber SAPHIR, Atmos. Chem. Phys., 5, 493-503,
- 723 https://doi.org/10.5194/acp-5-493-2005, 2005.
- Boucher, O., Randall, D., Artaxo, P., Bretherton, C., Feingold, G., Forster, P., Zhang, X. Y.: Clouds and
- aerosols, Cambridge University Press, Cambridge, UK, 2013.
- 726 Bruggemann, M., Xu, R., Tilgner, A., Kwong, K. C., Mutzel, A., Poon, H. Y., Herrmann, H.:
- 727 Organosulfates in Ambient Aerosol: State of Knowledge and Future Research Directions on
- 728 Formation, Abundance, Fate, and Importance, Environ Sci Technol, 54, 3767-3782,
- 729 https://doi.org/10.1021/acs.est.9b06751, 2020.
- 730 Canagaratna, M. R., Onasch, T. B., Wood, E. C., Herndon, S. C., Jayne, J. T., Cross, E. S., Worsnop, D.
- 731 R.: Evolution of Vehicle Exhaust Particles in the Atmosphere, Journal of the Air & Waste
- 732 Management Association, 60, 1192-1203, https://doi.org/10.3155/1047-3289.60.10.1192, 2010.
- Canagaratna, M. R., Jimenez, J. L., Kroll, J. H., Chen, Q., Kessler, S. H., Massoli, P., Worsnop, D. R.:
- 734 Elemental ratio measurements of organic compounds using aerosol mass spectrometry:
- characterization, improved calibration, and implications, Atmos. Chem. Phys., 15, 253-272,
- 736 https://doi.org/10.5194/acp-15-253-2015, 2015.
- 737 Canonaco, F., Slowik, J. G., Baltensperger, U., and Prévôt, A. S. H.: Seasonal differences in
- 738 oxygenated organic aerosol composition: implications for emissions sources and factor analysis,
- 739 Atmos Chem Phys, 15, 6993-7002, https://doi.org/10.5194/acp-15-6993-2015, 2015.
- 740 Canonaco, F., Crippa, M., Slowik, J. G., Baltensperger, U., and Prévôt, A. S. H.: SoFi, an IGOR-based
- 741 interface for the efficient use of the generalized multilinear engine (ME-2) for the source
- 742 apportionment: ME-2 application to aerosol mass spectrometer data, Atmos. Meas. Tech., 6, 3649-
- 743 3661, https://doi.org/10.5194/amt-6-3649-2013, 2013.

- Charlson, R. J., Lovelock, J. E., Andreae, M. O., and Warren, S. G.: Oceanic phytoplankton,
- atmospheric sulphur, cloud albedo and climate, Nature, 326, 655-661,
- 746 https://doi.org/10.1038/326655a0, 1987.
- 747 Chen, Q., Farmer, D. K., Rizzo, L. V., Pauliquevis, T., Kuwata, M., Karl, T. G., Martin, S. T.: Submicron
- 748 particle mass concentrations and sources in the Amazonian wet season (AMAZE-08), Atmos Chem
- 749 Phys, 15, 3687-3701, https://doi.org/10.5194/acp-15-3687-2015, 2015.
- 750 Chen, Y., Xu, L., Humphry, T., Hettiyadura, A. P. S., Ovadnevaite, J., Huang, S., Ng, N. L.: Response of
- 751 the Aerodyne Aerosol Mass Spectrometer to Inorganic Sulfates and Organosulfur Compounds:
- 752 Applications in Field and Laboratory Measurements, Environ Sci Technol, 53, 5176-5186,
- 753 <u>https://doi.org/10.1021/acs.est.9b00884</u>, 2019.
- 754 Cheng, Y., Ma, Y., and Hu, D.: Tracer-based source apportioning of atmospheric organic carbon and
- the influence of anthropogenic emissions on secondary organic aerosol formation in Hong Kong,
- 756 Atmos. Chem. Phys., 21, 10589-10608, https://doi.org/10.5194/acp-21-10589-2021, 2021.
- 757 Cho, C., Hofzumahaus, A., Fuchs, H., Dorn, H.-P., Glowania, M., Holland, F., Novelli, A.:
- 758 Characterization of a chemical modulation reactor (CMR) for the measurement of atmospheric
- 759 concentrations of hydroxyl radicals with a laser-induced fluorescence instrument, Atmospheric
- 760 Measurement Techniques, 14, 1851-1877, https://doi.org/10.5194/amt-14-1851-2021, 2021.
- 761 Cho, C., Fuchs, H., Hofzumahaus, A., Holland, F., Bloss, W. J., Bohn, B., Novelli, A.: Experimental
- 762 chemical budgets of OH, HO2, and RO2 radicals in rural air in western Germany during the JULIAC
- 763 campaign 2019, Atmos. Chem. Phys., 23, 2003-2033, https://doi.org/10.5194/acp-23-2003-2023,
- 764 2023.
- Coggon, M. M., Veres, P. R., Yuan, B., Koss, A., Warneke, C., Gilman, J. B., de Gouw, J. A.: Emissions of
- 766 nitrogen-containing organic compounds from the burning of herbaceous and arboraceous biomass:
- 767 Fuel composition dependence and the variability of commonly used nitrile tracers, Geophysical
- 768 Research Letters, 43, 9903-9912, https://doi.org/https://doi.org/10.1002/2016GL070562, 2016.
- 769 Crippa, M., DeCarlo, P. F., Slowik, J. G., Mohr, C., Heringa, M. F., Chirico, R., Baltensperger, U.:
- 770 Wintertime aerosol chemical composition and source apportionment of the organic fraction in the
- 771 metropolitan area of Paris, Atmos Chem Phys, 13, 961-981, https://doi.org/10.5194/acp-13-961-
- 772 **2013**, 2013.
- 773 Crippa, M., Canonaco, F., Lanz, V. A., Äijälä, M., Allan, J. D., Carbone, S., Prévôt, A. S. H.: Organic
- aerosol components derived from 25 AMS data sets across Europe using a consistent ME-2 based
- source apportionment approach, Atmos. Chem. Phys., 14, 6159-6176, https://doi.org/10.5194/acp-
- 776 14-6159-2014, 2014.
- 777 Cross, E. S., Slowik, J. G., Davidovits, P., Allan, J. D., Worsnop, D. R., Jayne, J. T., Onasch, T. B.:
- 778 Laboratory and Ambient Particle Density Determinations using Light Scattering in Conjunction with
- 779 Aerosol Mass Spectrometry, Aerosol Sci Tech, 41, 343-359,
- 780 https://doi.org/10.1080/02786820701199736, 2007.
- Dai, Q., Schulze, B. C., Bi, X., Bui, A. A. T., Guo, F., Wallace, H. W., Griffin, R. J.: Seasonal differences in
- formation processes of oxidized organic aerosol near Houston, TX, Atmos Chem Phys, 19, 9641-9661,
- 783 <u>https://doi.org/10.5194/acp-19-9641-2019</u>, 2019.
- Debevec, C., Sauvage, S., Gros, V., Salameh, T., Sciare, J., Dulac, F., and Locoge, N.: Seasonal variation
- and origins of volatile organic compounds observed during 2 years at a western Mediterranean
- remote background site (Ersa, Cape Corsica), Atmos. Chem. Phys., 21, 1449-1484,
- 787 https://doi.org/10.5194/acp-21-1449-2021, 2021.
- Debevec, C., Sauvage, S., Gros, V., Sciare, J., Pikridas, M., Stavroulas, I., Locoge, N.: Origin and
- 789 variability in volatile organic compounds observed at an Eastern Mediterranean background site
- 790 (Cyprus), Atmos. Chem. Phys., 17, 11355-11388, https://doi.org/10.5194/acp-17-11355-2017, 2017.
- 791 DeCarlo, P. F., Ulbrich, I. M., Crounse, J., de Foy, B., Dunlea, E. J., Aiken, A. C., Jimenez, J. L.:
- 792 Investigation of the sources and processing of organic aerosol over the Central Mexican Plateau from
- 793 aircraft measurements during MILAGRO, Atmos Chem Phys, 10, 5257-5280,
- 794 <u>https://doi.org/10.5194/acp-10-5257-2010, 2010.</u>

- 795 Desai, N. S., Moore, A. C., Mouat, A. P., Liang, Y., Xu, T., Takeuchi, M., Kaiser, J.: Impact of Heatwaves
- 796 and Declining NOx on Nocturnal Monoterpene Oxidation in the Urban Southeastern United States,
- Journal of Geophysical Research: Atmospheres, 129, e2024JD041482,
- 798 https://doi.org/https://doi.org/10.1029/2024JD041482, 2024.
- 799 Dockery, D. W. and Stone, P. H.: Cardiovascular Risks from Fine Particulate Air Pollution, New
- 800 England Journal of Medicine, 356, 511-513, https://doi.org/10.1056/NEJMe068274, 2007.
- 801 Dockery, D. W., Pope, C. A., Xu, X., Spengler, J. D., Ware, J. H., Fay, M. E., Speizer, F. E.: An Association
- between Air Pollution and Mortality in Six U.S. Cities, New England Journal of Medicine, 329, 1753-
- 803 1759, https://doi.org/10.1056/NEJM199312093292401, 1993.
- Fanourgakis, G. S., Kanakidou, M., Nenes, A., Bauer, S. E., Bergman, T., Carslaw, K. S., Yu, F.:
- 805 Evaluation of global simulations of aerosol particle and cloud condensation nuclei number, with
- implications for cloud droplet formation, Atmos. Chem. Phys., 19, 8591-8617,
- 807 https://doi.org/10.5194/acp-19-8591-2019, 2019.
- 808 Farmer, D. K., Matsunaga, A., Docherty, K. S., Surratt, J. D., Seinfeld, J. H., Ziemann, P. J., and
- 309 Jimenez, J. L.: Response of an aerosol mass spectrometer to organonitrates and organosulfates and
- 810 implications for atmospheric chemistry, Proc Natl Acad Sci U S A, 107, 6670-6675,
- 811 https://doi.org/10.1073/pnas.0912340107, 2010.
- 812 Faust, J. A., Wong, J. P. S., Lee, A. K. Y., and Abbatt, J. P. D.: Role of Aerosol Liquid Water in
- 813 Secondary Organic Aerosol Formation from Volatile Organic Compounds, Environ Sci Technol, 51,
- 814 1405-1413, https://doi.org/10.1021/acs.est.6b04700, 2017.
- 815 Florou, K., Papanastasiou, D. K., Pikridas, M., Kaltsonoudis, C., Louvaris, E., Gkatzelis, G. I., Pandis, S.
- 816 N.: The contribution of wood burning and other pollution sources to wintertime organic aerosol
- levels in two Greek cities, Atmos Chem Phys, 17, 3145-3163, https://doi.org/10.5194/acp-17-3145-
- 818 <u>2017</u>, 2017.
- 819 Fountoukis, C. and Nenes, A.: ISORROPIA II: a computationally efficient thermodynamic equilibrium
- 820 model for $K^+-Ca^{2+}-Mg^{2+}-NH_4^+-Na^+-SO_4^{2-}-NO_3^--Cl^--H_2O$ aerosols, Atmos. Chem. Phys., 7, 4639-4659,
- 821 https://doi.org/10.5194/acp-7-4639-2007, 2007.
- Fry, J. L., Kiendler-Scharr, A., Rollins, A. W., Wooldridge, P. J., Brown, S. S., Fuchs, H., Cohen, R. C.:
- 823 Organic nitrate and secondary organic aerosol yield from NO₃ oxidation of β-pinene evaluated using
- a gas-phase kinetics/aerosol partitioning model, Atmos. Chem. Phys., 9, 1431-1449,
- 825 https://doi.org/10.5194/acp-9-1431-2009, 2009.
- 826 Fry, J. L., Draper, D. C., Zarzana, K. J., Campuzano-Jost, P., Day, D. A., Jimenez, J. L., Grossberg, N.:
- Observations of gas- and aerosol-phase organic nitrates at BEACHON-RoMBAS 2011, Atmos. Chem.
- 828 Phys., 13, 8585-8605, https://doi.org/10.5194/acp-13-8585-2013, 2013.
- 829 Fuchs, H., Novelli, A., Rolletter, M., Hofzumahaus, A., Pfannerstill, E. Y., Kessel, S., Wahner, A.:
- 830 Comparison of OH reactivity measurements in the atmospheric simulation chamber SAPHIR, Atmos.
- 831 Meas. Tech., 10, 4023-4053, https://doi.org/10.5194/amt-10-4023-2017, 2017.
- 832 Ge, X. L., Zhang, Q., Sun, Y. L., Ruehl, C. R., and Setyan, A.: Effect of aqueous-phase processing on
- 833 aerosol chemistry and size distributions in Fresno, California, during wintertime, Environmental
- 834 Chemistry, 9, 221-235, https://doi.org/10.1071/en11168, 2012.
- Guo, H., Xu, L., Bougiatioti, A., Cerully, K. M., Capps, S. L., Hite Jr, J. R., Weber, R. J.: Fine-particle
- water and pH in the southeastern United States, Atmos. Chem. Phys., 15, 5211-5228,
- 837 https://doi.org/10.5194/acp-15-5211-2015, 2015.
- Hass-Mitchell, T., Joo, T., Rogers, M., Nault, B. A., Soong, C., Tran, M., Gentner, D. R.: Increasing
- 839 Contributions of Temperature-Dependent Oxygenated Organic Aerosol to Summertime Particulate
- 840 Matter in New York City, ACS ES&T Air, 1, 113-128, https://doi.org/10.1021/acsestair.3c00037, 2024.
- Hayes, P. L., Ortega, A. M., Cubison, M. J., Froyd, K. D., Zhao, Y., Cliff, S. S., Jimenez, J. L.: Organic
- aerosol composition and sources in Pasadena, California, during the 2010 CalNex campaign, Journal
- of Geophysical Research: Atmospheres, 118, 9233-9257, https://doi.org/10.1002/jgrd.50530, 2013.

- Hildebrandt, L., Engelhart, G. J., Mohr, C., Kostenidou, E., Lanz, V. A., Bougiatioti, A., Pandis, S. N.:
- 845 Aged organic aerosol in the Eastern Mediterranean: the Finokalia Aerosol Measurement Experiment-
- 2008, Atmos Chem Phys, 10, 4167-4186, https://doi.org/10.5194/acp-10-4167-2010, 2010.
- Hoyle, C. R., Berntsen, T., Myhre, G., and Isaksen, I. S. A.: Secondary organic aerosol in the global
- aerosol chemical transport model Oslo CTM2, Atmos. Chem. Phys., 7, 5675-5694,
- 849 https://doi.org/10.5194/acp-7-5675-2007, 2007.
- 850 Hu, W. W., Hu, M., Yuan, B., Jimenez, J. L., Tang, Q., Peng, J. F., He, L. Y.: Insights on organic aerosol
- aging and the influence of coal combustion at a regional receptor site of central eastern China,
- 852 Atmos. Chem. Phys., 13, 10095-10112, https://doi.org/10.5194/acp-13-10095-2013, 2013.
- Hu, W. W., Campuzano-Jost, P., Palm, B. B., Day, D. A., Ortega, A. M., Hayes, P. L., Jimenez, J. L.:
- 854 Characterization of a real-time tracer for isoprene epoxydiols-derived secondary organic aerosol
- 855 (IEPOX-SOA) from aerosol mass spectrometer measurements, Atmos Chem Phys, 15, 11807-11833,
- 856 https://doi.org/10.5194/acp-15-11807-2015, 2015.
- Huang, D. D., Li, Y. J., Lee, B. P., and Chan, C. K.: Analysis of Organic Sulfur Compounds in
- 858 Atmospheric Aerosols at the HKUST Supersite in Hong Kong Using HR-ToF-AMS, Environ Sci Technol,
- 49, 3672-3679, https://doi.org/10.1021/es5056269, 2015.
- 860 Huang, L., Liu, T., and Grassian, V. H.: Radical-Initiated Formation of Aromatic Organosulfates and
- Sulfonates in the Aqueous Phase, Environ Sci Technol, 54, 11857-11864,
- 862 https://doi.org/10.1021/acs.est.0c05644, 2020.
- Huang, S., Poulain, L., van Pinxteren, D., van Pinxteren, M., Wu, Z., Herrmann, H., and Wiedensohler,
- 864 A.: Latitudinal and Seasonal Distribution of Particulate MSA over the Atlantic using a Validated
- Quantification Method with HR-ToF-AMS, Environ Sci Technol, 51, 418-426,
- 866 https://doi.org/10.1021/acs.est.6b03186, 2017.
- 867 Insight, B.: German sugar manufacturer Pfeifer & Langen converts to biomass boilers, 2023.
- Jimenez, J. L., Canagaratna, M. R., Donahue, N. M., Prevot, A. S., Zhang, Q., Kroll, J. H., Worsnop, D.
- 869 R.: Evolution of organic aerosols in the atmosphere, Science, 326, 1525-1529,
- 870 https://doi.org/10.1126/science.1180353, 2009.
- 871 Kharuk, V. I. and Ponomarev, E.: Spatiotemporal characteristics of wildfire frequency and relative
- area burned in larch-dominated forests of Central Siberia, Russian Journal of Ecology, 48, 507-512,
- 873 https://doi.org/10.1134/S1067413617060042, 2017.
- Kiendler-Scharr, A., Mensah, A. A., Friese, E., Topping, D., Nemitz, E., Prevot, A. S. H., Wu, H. C.:
- Ubiquity of organic nitrates from nighttime chemistry in the European submicron aerosol,
- 876 Geophysical Research Letters, 43, 7735-7744, https://doi.org/10.1002/2016gl069239, 2016.
- Kodros, J. K., Papanastasiou, D. K., Paglione, M., Masiol, M., Squizzato, S., Florou, K., Pandis, S. N.:
- 878 Rapid dark aging of biomass burning as an overlooked source of oxidized organic aerosol, Proc Natl
- 879 Acad Sci U S A, 117, 33028-33033, https://doi.org/10.1073/pnas.2010365117, 2020.
- Kostenidou, E., Lee, B.-H., Engelhart, G. J., Pierce, J. R., and Pandis, S. N.: Mass Spectra
- 881 Deconvolution of Low, Medium, and High Volatility Biogenic Secondary Organic Aerosol, Environ Sci
- 882 Technol, 43, 4884-4889, https://doi.org/10.1021/es803676g, 2009.
- 883 Kostenidou, E., Florou, K., Kaltsonoudis, C., Tsiflikiotou, M., Vratolis, S., Eleftheriadis, K., and Pandis,
- 884 S. N.: Sources and chemical characterization of organic aerosol during the summer in the eastern
- 885 Mediterranean, Atmos Chem Phys, 15, 11355-11371, https://doi.org/10.5194/acp-15-11355-2015,
- 886 2015.
- Lee, B. H., Mohr, C., Lopez-Hilfiker, F. D., Lutz, A., Hallquist, M., Lee, L., Thornton, J. A.: Highly
- 888 functionalized organic nitrates in the southeast United States: Contribution to secondary organic
- aerosol and reactive nitrogen budgets, Proc Natl Acad Sci U S A, 113, 1516-1521,
- 890 https://doi.org/10.1073/pnas.1508108113, 2016.
- 891 Lelieveld, J., Evans, J. S., Fnais, M., Giannadaki, D., and Pozzer, A.: The contribution of outdoor air
- 892 pollution sources to premature mortality on a global scale, Nature, 525, 367-371,
- 893 https://doi.org/10.1038/nature15371, 2015.

- 894 Li, J., Pósfai, M., Hobbs, P. V., and Buseck, P. R.: Individual aerosol particles from biomass burning in
- southern Africa: 2, Compositions and aging of inorganic particles, Journal of Geophysical Research:
- 896 Atmospheres, 108, https://doi.org/10.1029/2002JD002310, 2003.
- Li, Y. J., Lee, B. P., Su, L., Fung, J. C. H., and Chan, C. K.: Seasonal characteristics of fine particulate
- 898 matter (PM) based on high-resolution time-of-flight aerosol mass spectrometric (HR-ToF-AMS)
- measurements at the HKUST Supersite in Hong Kong, Atmos Chem Phys, 15, 37-53,
- 900 https://doi.org/10.5194/acp-15-37-2015, 2015.
- 901 Liggio, J. and Li, S.-M.: Reactive uptake of pinonaldehyde on acidic aerosols, Journal of Geophysical
- 902 Research: Atmospheres, 111, https://doi.org/10.1029/2005JD006978, 2006.
- Lipiäinen, S., Kuparinen, K., Sermyagina, E., and Vakkilainen, E.: Pulp and paper industry in energy
- transition: Towards energy-efficient and low carbon operation in Finland and Sweden, Sustainable
- 905 Production and Consumption, 29, 421-431, https://doi.org/10.1016/j.spc.2021.10.029, 2022.
- Liu, L., Hohaus, T., Franke, P., Lange, A. C., Tillmann, R., Fuchs, H., Kiendler-Scharr, A.: Seasonal
- 907 Comparison of the Chemical Composition and Source Apportionment of Aerosols during the Year-
- 908 Long JULIAC Campaign, Doctoral Thesis, Energy & Environment, University of Wuppertal,
- 909 Forschungszentrum Jülich GmbH, https://juser.fz-juelich.de/record/916580, 2022.
- 910 Liu, L., Hohaus, T., Franke, P., Lange, A. C., Tillmann, R., Fuchs, H., Kiendler-Scharr, A.: Observational
- 911 evidence reveals the significance of nocturnal chemistry in seasonal secondary organic aerosol
- 912 formation, npj Climate and Atmospheric Science, 7, 207, https://doi.org/10.1038/s41612-024-
- 913 00747-6, 2024.
- 914 Ma, M., Gao, Y., Wang, Y., Zhang, S., Leung, L. R., Liu, C., Gao, H.: Substantial ozone enhancement
- over the North China Plain from increased biogenic emissions due to heat waves and land cover in
- 916 summer 2017, Atmos. Chem. Phys., 19, 12195-12207, https://doi.org/10.5194/acp-19-12195-2019,
- 917 2019.
- 918 Matzarakis, A., Laschewski, G., and Muthers, S.: The Heat Health Warning System in Germany-
- 919 Application and Warnings for 2005 to 2019, Atmosphere, 11,
- 920 https://doi.org/10.3390/atmos11020170, 2020.
- 921 McFiggans, G., Mentel, T. F., Wildt, J., Pullinen, I., Kang, S., Kleist, E., Kiendler-Scharr, A.: Secondary
- 922 organic aerosol reduced by mixture of atmospheric vapours, Nature, 565, 587-593,
- 923 https://doi.org/10.1038/s41586-018-0871-y, 2019.
- 924 Meng, X., Wu, Z., Chen, J., Qiu, Y., Zong, T., Song, M., Hu, M.: Particle phase state and aerosol liquid
- 925 water greatly impact secondary aerosol formation: insights into phase transition and its role in haze
- 926 events, Atmos. Chem. Phys., 24, 2399-2414, https://doi.org/10.5194/acp-24-2399-2024, 2024.
- 927 Mentel, T. F., Kleist, E., Andres, S., Dal Maso, M., Hohaus, T., Kiendler-Scharr, A., Wildt, J.: Secondary
- aerosol formation from stress-induced biogenic emissions and possible climate feedbacks, Atmos.
- 929 Chem. Phys., 13, 8755-8770, https://doi.org/10.5194/acp-13-8755-2013, 2013.
- 930 Middlebrook, A. M., Bahreini, R., Jimenez, J. L., and Canagaratna, M. R.: Evaluation of Composition-
- 931 Dependent Collection Efficiencies for the Aerodyne Aerosol Mass Spectrometer using Field Data,
- 932 Aerosol Sci Tech, 46, 258-271, https://doi.org/10.1080/02786826.2011.620041, 2012.
- 933 Mohr, C., DeCarlo, P. F., Heringa, M. F., Chirico, R., Slowik, J. G., Richter, R., Prévôt, A. S. H.:
- 934 Identification and quantification of organic aerosol from cooking and other sources in Barcelona
- using aerosol mass spectrometer data, Atmos Chem Phys, 12, 1649-1665,
- 936 https://doi.org/10.5194/acp-12-1649-2012, 2012.
- 937 Myhre, G., Samset, B. H., Schulz, M., Balkanski, Y., Bauer, S., Berntsen, T. K., Zhou, C.: Radiative
- 938 forcing of the direct aerosol effect from AeroCom Phase II simulations, Atmos. Chem. Phys., 13,
- 939 1853-1877, https://doi.org/10.5194/acp-13-1853-2013, 2013.
- 940 Ng, N. L., Canagaratna, M. R., Jimenez, J. L., Chhabra, P. S., Seinfeld, J. H., and Worsnop, D. R.:
- 941 Changes in organic aerosol composition with aging inferred from aerosol mass spectra,
- 942 https://doi.org/10.5194/acpd-11-7095-2011, 2011.

- 943 Ng, N. L., Kwan, A. J., Surratt, J. D., Chan, A. W. H., Chhabra, P. S., Sorooshian, A., Seinfeld, J. H.:
- 944 Secondary organic aerosol (SOA) formation from reaction of isoprene with nitrate radicals (NO₃),
- 945 Atmos. Chem. Phys., 8, 4117-4140, https://doi.org/10.5194/acp-8-4117-2008, 2008.
- Ng, N. L., Canagaratna, M. R., Zhang, Q., Jimenez, J. L., Tian, J., Ulbrich, I. M., Worsnop, D. R.: Organic
- 947 aerosol components observed in Northern Hemispheric datasets from Aerosol Mass Spectrometry,
- 948 Atmos. Chem. Phys., 10, 4625-4641, https://doi.org/10.5194/acp-10-4625-2010, 2010.
- 949 Ng, N. L., Brown, S. S., Archibald, A. T., Atlas, E., Cohen, R. C., Crowley, J. N., Zaveri, R. A.: Nitrate
- 950 radicals and biogenic volatile organic compounds: oxidation, mechanisms, and organic aerosol,
- 951 Atmos. Chem. Phys., 17, 2103-2162, https://doi.org/10.5194/acp-17-2103-2017, 2017.
- 952 Otu-Larbi, F., Bolas, C. G., Ferracci, V., Staniaszek, Z., Jones, R. L., Malhi, Y., Ashworth, K.: Modelling
- the effect of the 2018 summer heatwave and drought on isoprene emissions in a UK woodland, Glob
- 954 Chang Biol, 26, 2320-2335, https://doi.org/10.1111/gcb.14963, 2020.
- 955 Paatero, P.: The Multilinear Engine: A Table-Driven, Least Squares Program for Solving Multilinear
- 956 Problems, including the n-Way Parallel Factor Analysis Model, Journal of Computational and
- 957 Graphical Statistics, 8, 854-888, https://doi.org/10.2307/1390831, 1999.
- Paatero, P. and Hopke, P. K.: Discarding or downweighting high-noise variables in factor analytic
- 959 models, Analytica Chimica Acta, 490, 277-289, https://doi.org/10.1016/S0003-2670(02)01643-4,
- 960 2003.
- 961 Parworth, C., Fast, J., Mei, F., Shippert, T., Sivaraman, C., Tilp, A., Zhang, Q.: Long-term measurements
- of submicrometer aerosol chemistry at the Southern Great Plains (SGP) using an Aerosol Chemical
- 963 Speciation Monitor (ACSM), Atmospheric Environment, 106, 43-55,
- 964 https://doi.org/10.1016/j.atmosenv.2015.01.060, 2015.
- Petit, J. E., Amodeo, T., Meleux, F., Bessagnet, B., Menut, L., Grenier, D., Favez, O.: Characterising an
- 966 intense PM pollution episode in March 2015 in France from multi-site approach and near real time
- 967 data: Climatology, variabilities, geographical origins and model evaluation, Atmospheric
- 968 Environment, 155, 68-84, https://doi.org/10.1016/j.atmosenv.2017.02.012, 2017.
- 969 Pope, C. A. and Dockery, D. W.: Health Effects of Fine Particulate Air Pollution: Lines that Connect,
- 970 Journal of the Air & Waste Management Association, 56, 709-742,
- 971 https://doi.org/10.1080/10473289.2006.10464485, 2006.
- 972 Pye, H. O. T., Chan, A. W. H., Barkley, M. P., and Seinfeld, J. H.: Global modeling of organic aerosol:
- 973 the importance of reactive nitrogen (NO_x and NO₃), Atmos Chem Phys, 10, 11261-11276,
- 974 https://doi.org/10.5194/acp-10-11261-2010, 2010.
- 975 Raatikainen, T., Vaattovaara, P., Tiitta, P., Miettinen, P., Rautiainen, J., Ehn, M., Worsnop, D. R.:
- 976 Physicochemical properties and origin of organic groups detected in boreal forest using an aerosol
- 977 mass spectrometer, Atmos Chem Phys, 10, 2063-2077, https://doi.org/10.5194/acp-10-2063-2010,
- 978 2010.
- 979 Ramanathan, V., Crutzen, P. J., Kiehl, J. T., and Rosenfeld, D.: Aerosols, Climate, and the Hydrological
- 980 Cycle, Science, 294, 2119, https://doi.org/10.1126/science.1064034, 2001.
- Riva, M., Heikkinen, L., Bell, D. M., Peräkylä, O., Zha, Q., Schallhart, S., Ehn, M.: Chemical
- transformations in monoterpene-derived organic aerosol enhanced by inorganic composition, npj
- 983 Climate and Atmospheric Science, 2, https://doi.org/10.1038/s41612-018-0058-0, 2019.
- 984 Russell, M.: Predicting secondary organic aerosol formation rates in southeast Texas, Journal of
- 985 Geophysical Research, 110, https://doi.org/10.1029/2004jd004722, 2005.
- 986 Saarikoski, S., Carbone, S., Decesari, S., Giulianelli, L., Angelini, F., Canagaratna, M., Worsnop, D.:
- 987 Chemical characterization of springtime submicrometer aerosol in Po Valley, Italy, Atmos Chem
- 988 Phys, 12, 8401-8421, https://doi.org/10.5194/acp-12-8401-2012, 2012.
- 989 Schlag, P., Kiendler-Scharr, A., Blom, M. J., Canonaco, F., Henzing, J. S., Moerman, M., Holzinger, R.:
- 990 Aerosol source apportionment from 1-year measurements at the CESAR tower in Cabauw, the
- 991 Netherlands, Atmos Chem Phys, 16, 8831-8847, https://doi.org/10.5194/acp-16-8831-2016, 2016.

- 992 Schlag, P., Rubach, F., Mentel, T. F., Reimer, D., Canonaco, F., Henzing, J. S., Kiendler-Scharr, A.:
- 993 Ambient and laboratory observations of organic ammonium salts in PM1, Faraday Discuss, 200, 331-
- 994 351, https://doi.org/10.1039/c7fd00027h, 2017.
- 995 Schmale, J., Schneider, J., Nemitz, E., Tang, Y. S., Dragosits, U., Blackall, T. D., Braban, C. F.: Sub-
- 996 Antarctic marine aerosol: dominant contributions from biogenic sources, Atmos Chem Phys, 13,
- 997 8669-8694, https://doi.org/10.5194/acp-13-8669-2013, 2013.
- 998 Schueneman, M. K., Nault, B. A., Campuzano-Jost, P., Jo, D. S., Day, D. A., Schroder, J. C., Jimenez, J.
- 999 L.: Aerosol pH indicator and organosulfate detectability from aerosol mass spectrometry
- 1000 measurements, Atmospheric Measurement Techniques, 14, 2237-2260,
- 1001 https://doi.org/10.5194/amt-14-2237-2021, 2021.
- Seibert, P., Kromp-Kolb, H., Baltensperger, U., Jost, D. T., and Schwikowski, M.: Air Pollution
- 1003 Modeling and Its Application X, 1994.
- Simoneit, B. R. T., Schauer, J. J., Nolte, C. G., Oros, D. R., Elias, V. O., Fraser, M. P., Cass, G. R.:
- 1005 Levoglucosan, a tracer for cellulose in biomass burning and atmospheric particles, Atmospheric
- 1006 Environment, 33, 173-182, https://doi.org/10.1016/S1352-2310(98)00145-9, 1999.
- 1007 Stein, A. F., Draxler, R. R., Rolph, G. D., Stunder, B. J., Cohen, M. D., and Ngan, F.: NOAA's HYSPLIT
- 1008 atmospheric transport and dispersion modeling system, Bulletin of the American Meteorological
- 1009 Society, 96, 2059-2077, https://doi.org/10.1175/BAMS-D-14-00110.1, 2015.
- 1010 Sun, Y., Du, W., Fu, P., Wang, Q., Li, J., Ge, X., Wang, Z.: Primary and secondary aerosols in Beijing in
- 1011 winter: sources, variations and processes, Atmos Chem Phys, 16, 8309-8329,
- 1012 https://doi.org/10.5194/acp-16-8309-2016, 2016.
- Sun, Y. L., Zhang, Q., Schwab, J. J., Yang, T., Ng, N. L., and Demerjian, K. L.: Factor analysis of
- 1014 combined organic and inorganic aerosol mass spectra from high resolution aerosol mass
- spectrometer measurements, Atmos Chem Phys, 12, 8537-8551, https://doi.org/10.5194/acp-12-
- 1016 <u>8537-2012</u>, 2012.
- 1017 Tan, S., Zhang, X., Lian, Y., Chen, X., Yin, S., Du, L., and Ge, M.: OH Group Orientation Leads to
- 1018 Organosulfate Formation at the Liquid Aerosol Surface, Journal of the American Chemical Society,
- 1019 144, 16953-16964, https://doi.org/10.1021/jacs.2c05807, 2022a.
- Tan, Z., Fuchs, H., Hofzumahaus, A., Bloss, W. J., Bohn, B., Cho, C., Sommariva, R.: Seasonal variation
- in nitryl chloride and its relation to gas-phase precursors during the JULIAC campaign in Germany,
- 1022 Atmos. Chem. Phys., 22, 13137-13152, https://doi.org/10.5194/acp-22-13137-2022, 2022b.
- Tao, J., Gao, J., Zhang, L., Zhang, R., Che, H., Zhang, Z., Hsu, S. C.: PM_{2.5} pollution in a megacity of
- southwest China: source apportionment and implication, Atmos. Chem. Phys., 14, 8679-8699,
- 1025 https://doi.org/10.5194/acp-14-8679-2014, 2014.
- 1026 Wagner, N. L., Dubé, W. P., Washenfelder, R. A., Young, C. J., Pollack, I. B., Ryerson, T. B., and Brown,
- 1027 S. S.: Diode laser-based cavity ring-down instrument for NO₃, N₂O₅, NO, NO₂ and O₃ from aircraft,
- 1028 Atmos. Meas. Tech., 4, 1227-1240, https://doi.org/10.5194/amt-4-1227-2011, 2011.
- Wang, Y., Zhao, Y., Wang, Y., Yu, J.-Z., Shao, J., Liu, P., Xiao, H.: Organosulfates in atmospheric
- aerosols in Shanghai, China: seasonal and interannual variability, origin, and formation mechanisms,
- 1031 Atmos Chem Phys, 21, 2959-2980, https://doi.org/10.5194/acp-21-2959-2021, 2021a.
- Wang, Y., Zhao, Y., Wang, Y., Yu, J. Z., Shao, J., Liu, P., Xiao, H.: Organosulfates in atmospheric
- aerosols in Shanghai, China: seasonal and interannual variability, origin, and formation mechanisms,
- 1034 Atmos. Chem. Phys., 21, 2959-2980, https://doi.org/10.5194/acp-21-2959-2021, 2021b.
- 1035 Xu, L., Suresh, S., Guo, H., Weber, R. J., and Ng, N. L.: Aerosol characterization over the southeastern
- 1036 United States using high-resolution aerosol mass spectrometry: spatial and seasonal variation of
- aerosol composition and sources with a focus on organic nitrates, Atmos. Chem. Phys., 15, 7307-
- 1038 7336, https://doi.org/10.5194/acp-15-7307-2015, 2015a.
- 1039 Xu, L., Guo, H., Boyd, C. M., Klein, M., Bougiatioti, A., Cerully, K. M., Ng, N. L.: Effects of
- 1040 anthropogenic emissions on aerosol formation from isoprene and monoterpenes in the
- southeastern United States, Proc Natl Acad Sci U S A, 112, E4506-4507,
- 1042 https://doi.org/10.1073/pnas.1512277112, 2015b.

- 1043 Xu, L., Guo, H., Boyd, C. M., Klein, M., Bougiatioti, A., Cerully, K. M., Ng, N. L.: Effects of
- anthropogenic emissions on aerosol formation from isoprene and monoterpenes in the
- southeastern United States, Proc Natl Acad Sci U S A, 112, 37-42,
- 1046 https://doi.org/10.1073/pnas.1417609112, 2015c.
- 1047 Yan, J. P., Jung, J. Y., Zhang, M. M., Xu, S. Q., Lin, Q., Zhao, S. H., and Chen, L. Q.: Significant
- 1048 Underestimation of Gaseous Methanesulfonic Acid (MSA) over Southern Ocean, Environ Sci Technol,
- 1049 53, 13064-13070, https://doi.org/10.1021/acs.est.9b05362, 2019.
- 1050 Yang, J.-R., Liu, A., and Long, B.: An unexpected feasible route for the formation of organosulfates by
- the gas phase reaction of sulfuric acid with acetaldehyde catalyzed by dimethylamine in the
- atmosphere, Environmental Science: Atmospheres, 3, 672-682,
- 1053 https://doi.org/10.1039/D2EA00159D, 2023.
- 1054 Yao, M., Zhao, Y., Hu, M., Huang, D., Wang, Y., Yu, J. Z., and Yan, N.: Multiphase Reactions between
- 1055 Secondary Organic Aerosol and Sulfur Dioxide: Kinetics and Contributions to Sulfate Formation and
- 1056 Aerosol Aging, Environmental Science & Technology Letters, 6, 768-774,
- 1057 https://doi.org/10.1021/acs.estlett.9b00657, 2019.
- 1058 Young, D. E., Kim, H., Parworth, C., Zhou, S., Zhang, X., Cappa, C. D., Zhang, Q.: Influences of emission
- sources and meteorology on aerosol chemistry in a polluted urban environment: results from
- 1060 DISCOVER-AQ California, Atmos. Chem. Phys., 16, 5427-5451, https://doi.org/10.5194/acp-16-5427-
- 1061 <u>2016</u>, 2016.
- 1062 Yu, J., Yan, C., Liu, Y., Li, X., Zhou, T., and Zheng, M.: Potassium: A Tracer for Biomass Burning in
- Beijing?, Aerosol and Air Quality Research, 18, 2447-2459,
- 1064 https://doi.org/10.4209/aaqr.2017.11.0536, 2018.
- Zhang, G., Yu, X., Yin, H., Feng, C., Ma, C., Sun, S., Liu, X.: Heatwave-amplified atmospheric oxidation
- in a multi-province border area in Xuzhou, China, Frontiers in Environmental Science, 12, 1496584,
- 1067 https://doi.org/10.3389/fenvs.2024.1496584, 2024.
- 1068 Zhang, Q., Jimenez, J. L., Canagaratna, M. R., Ulbrich, I. M., Ng, N. L., Worsnop, D. R., and Sun, Y.:
- 1069 Understanding atmospheric organic aerosols via factor analysis of aerosol mass spectrometry: a
- review, Anal Bioanal Chem, 401, 3045-3067, https://doi.org/10.1007/s00216-011-5355-y, 2011.
- 1071 Zhang, Q., Jimenez, J. L., Canagaratna, M. R., Allan, J. D., Coe, H., Ulbrich, I., Worsnop, D. R.: Ubiquity
- and dominance of oxygenated species in organic aerosols in anthropogenically-influenced Northern
- 1073 Hemisphere midlatitudes, Geophysical Research Letters, 34,
- 1074 https://doi.org/https://doi.org/10.1029/2007GL029979, 2007.
- 1075 Zhang, R., Jing, J., Tao, J., Hsu, S. C., Wang, G., Cao, J., Shen, Z.: Chemical characterization and source
- apportionment of PM_{2.5} in Beijing: seasonal perspective, Atmos. Chem. Phys., 13, 7053-7074,
- 1077 https://doi.org/10.5194/acp-13-7053-2013, 2013.
- 1078 Zhang, Y. J., Tang, L. L., Wang, Z., Yu, H. X., Sun, Y. L., Liu, D., Zhou, H. C.: Insights into characteristics,
- 1079 sources, and evolution of submicron aerosols during harvest seasons in the Yangtze River delta
- region, China, Atmos Chem Phys, 15, 1331-1349, https://doi.org/10.5194/acp-15-1331-2015, 2015.
- Zhou, S., Collier, S., Jaffe, D. A., Briggs, N. L., Hee, J., Sedlacek Iii, A. J., Zhang, Q.: Regional influence of
- 1082 wildfires on aerosol chemistry in the western US and insights into atmospheric aging of biomass
- burning organic aerosol, Atmos Chem Phys, 17, 2477-2493, https://doi.org/10.5194/acp-17-2477-
- 1084 **2017**, 2017.

- Zorn, S. R., Drewnick, F., Schott, M., Hoffmann, T., and Borrmann, S.: Characterization of the South
- 1086 Atlantic marine boundary layer aerosol using an aerodyne aerosol mass spectrometer, Atmos Chem
- 1087 Phys, 8, 4711-4728, https://doi.org/10.5194/acp-8-4711-2008, 2008.